Improved rule-based power distribution algorithm for hybrid battery storage systems and real-world validation

Lucas Koltermann[a,b,c]1, Mauricio Celi Cortés[a,b,c], Jan Figgener[a,b,c], Sebastian Zurmühlen[a,b,c], Dirk Uwe Sauer[a,b,c,d]

[a] *Institute for Power Electronics and Electrical Drives (ISEA), RWTH Aachen University, 52074 Aachen, Germany*
[b] *Institute for Power Generation and Storage Systems (PGS), E.ON ERC, RWTH Aachen University, 52074 Aachen, Germany*
[c] *Jülich Aachen Research Alliance, JARA-Energy, 52056 Aachen / 52425 Jülich, Germany*
[d] *Forschungszentrum Jülich GmbH, Institute of Energy and Climate Research Helmholtz-Institute Münster: Ionics in Energy Storage (IEK-12), 52425 Jülich, Germany*

* Corresponding author. Tel.: +49 241 80 49338.
E-mail address: lucas.koltermann@isea.rwth-aachen.de or batteries@isea.rwth-aachen.de

Abstract

Large-scale battery energy storage systems (BESS) can serve many applications and are already widely used for grid services. The rapidly growing BESS market and the recent interest in their deployment accentuate the need for safe, reliable, and highly available energy management systems (EMS) for automated control. However, the EMS and their integrated power distribution algorithms (PDA) can still be optimized to adapt various characteristics of the BESS. This study investigates a new version of a PDA with a particular focus on battery aging and system efficiency. The rule-based PDA has been validated on a 6 MW/7.5 MWh BESS system with five battery technologies providing frequency containment reserve to the German power grid. The results underline the PDA's capability to exploit the individual strengths of each battery technology. The PDA sets objectives for the state of charge, energy throughput, and power of the batteries to extend battery life. The distribution of energy throughputs among batteries can be selected in advance through the new implementation of the PDA. At the same time, the inverters are significantly less often activated and used in the optimal efficiency range, increasing the overall system efficiency to approximately 82 %. The optimized switching behavior leads to less frequent power switching between individual battery units and longer phases with more constant power. In addition, the operational efficiency of BESS can be improved by the choice of battery technology and the overall system layout on the hardware side. The improvements on the software side are only possible by increasing the overall power requests through multi-use operation by about 6 % compared to our benchmark test. The results can be used by BESS operators to increase operational profits due to longer battery life and fewer efficiency losses.

Keywords: battery storage system; field test; efficiency; benchmark test; power distribution algorithm

Nomenclature

Abbreviation	Description
BESS	Battery energy storage system
BMS	Battery management system
EMS	Energy management system
FCR	Frequency containment reserve
LFP	Lithium iron phosphate
LMO	Lithium manganese oxide
LTO	Lithium titanate oxide
M5BAT	Modular Multi-Megawatt Medium Voltage Battery Storage System
NCA	Lithium nickel cobalt aluminium
NMC	Lithium nickel manganese cobalt oxide
OCSM	Lead acid battery with liquid electrolyte
OPzV	Lead acid battery with gelled electrolyte
PbA	Lead acid battery
PCS	Power conversion system
PDA	Power distribution algorithm
RTE	Round-trip efficiency
SOC	State of charge
SPDA V.2022	Staged rule-based power distribution algorithm Version 2022
SPDA V.2023	Staged rule-based power distribution algorithm Version 2023 (improvements presented within this study)

1 Introduction

The ongoing energy transition towards renewable energy generation requires various energy storage technologies in the energy sector to ensure flexibility and grid stability in the future. The market for battery energy storage systems (BESS) has grown rapidly in the past years and is expected to grow further in the upcoming years [1–5]. Currently, BESS are used for front-of-the-meter applications such as grid services, spot market trading, grid boosting, grid voltage regulation, and island operation or behind-the-meter applications such as peak shaving, increase of self-consumption and uninterruptible power supply [2, 5–12]. Ancillary services are currently mostly served by large-scale BESS [3]. Due to the transition to more sustainable energy supply sources the need for faster ancillary services could arise in the near future. In [13], the response times of the modular multi-megawatt medium voltage battery storage system (M5BAT) components were evaluated, which now determines which other market applications can be served and where hardware upgrades need to be made before the market application requirements are met. An example is the enhanced frequency response in the UK market [14].

The energy management system (EMS) is the key tool of a BESS, allowing storage to provide this large variety of applications [15, 16]. The battery management system (BMS) can be a part of the EMS and ensures the safe operation of the battery units. Additional features for BESS can be deployed after commissioning, and the EMS can be improved via continuous software development. A power distribution algorithm (PDA) is an essential part of the EMS which is necessary to control a BESS with multiple battery units [17]. The PDA decides when to charge or discharge which battery unit. On the BESS side, the efficiency and utilization of the power conversion system (PCS) can be controlled, while on the battery side, the energy throughput, the C-rate, and the state of charge (SOC) are controlled by the PDA.

In the previous research on the PDA of the BESS M5BAT, the staged rule-based power distribution algorithm (SPDA) was introduced [17]. Building on previous research on the PDA of the BESS M5BAT [17], which is now refered to as Version 2022 (SPDA V.2022), we have continuously added features to the EMS and improved the PDA. As a result, the profitability of the BESS operation has been improved by increasing the lifetime and reliability of the system while reducing the energy losses. The proposed new version of the SPDA (SPDA V.2023) in this study allows for a significant reduction in inverter activations and includes advanced settings to improve the efficiency of the overall system. In addition, this study provides a deeper understanding of the capabilities of the PDA through a detailed analysis of the inverter and transformer efficiency curves. Cyclic battery load and energy throughput improvements are also presented. The functionality and effects of the new features of the PDA are verified through field tests on the BESS M5BAT under real conditions. For the classification of the BESS efficiencies, reference values from previous years and a benchmark test of the BESS M5BAT are used. The new features of the SPDA enable a more

stable and efficient operation of modular BESS compared to the SPDA V.2022 presented in [17].

2 Literature review

In this section, the state-of-the-art and current developments of EMS and PDAs are discussed. Since this work has a special focus on efficiency under consideration of battery aging, battery aging, and efficiency studies are summarized and discussed.

2.1 Energy management systems

An EMS is required to manage the reliable use of all battery units which compose a BESS. The control of the battery units of different battery technologies, as found in modular and hybrid BESS, is more complex, requiring advanced EMS [7, 10, 15, 17–20]. The PDA within the EMS has a direct influence on the battery load and usage time and thus an indirect influence on the battery aging, efficiency, and reliability [17]. Despite the market growth of BESS, the EMS, and PDAs are typically not disclosed by storage system manufacturers and operators in order to be competitive in the market [1, 17].

Research in the field of EMS is mainly focused on different applications and the description of methods for optimizing it for the different applications [21, 22]. In addition, EMS research provides simulations such as the simulation of EMS strategies according to the multi-agent theory for smoothing the peak loads of photovoltaics and wind power generation, according to Li and Zhang [23]. Moreover, Ngoc An and Quoc-Tuan [24] provide EMS simulations for the stabilization of a grid connected microgrid with BESS. They showed that their rule-based method is capable of minimizing the net power imports to the microgrid [24]. Multi-objective genetic algorithms were also used to optimize the EMS of a BESS in a microgrid [25]. However, this study lacks a real-world testing scenario [25].

The EMS development in SOC management strategies was shown by Marchgraber *et al.* [26]. The energy necessary for SOC-management could be reduced and by using a PDA compared to an equal power distribution the losses were reduced by about 60 % [26]. This helps to reduce costs which results in an increased profitability of BESS. However, the PDA was not investigated. Choi *et al.* [27] presented PDAs with different objectives such as the energy efficiency or the system availability. It was proposed to use a combination of both algorithms and to execute a efficiency test to improve the PDAs performance before using the algorithm in BESS [27]. Furthermore, power flow strategies were presented in a model and validated by lab-scale tests [28, 29]. In [30], further optimizations of their PDA were shown simulatively. For the target indicators of performance, service life and efficiency pareto-optimal solutions were identified successfully [30]. The iterative dynamic programming approach was chosen to find a global optimal PDA [31]. For frequency regulation services in Korea, Cho and Yun [32] could achieve efficiency increases with the help of a PDA. For a one-month simulation of a BESS with multiple battery units delivering frequency regulation services, the losses were cut by half by the PDA compared to a uniformly assigning power distribution [32]. PDA in field applications were investigated by Schimpe *et al.* [33] and in

[17]. In field tests the partial loads of power conversion system influence the BESS efficiency in a significant way [17, 33]. Therefore the no-load losses of the power conversion system a low partial load should be covered by as few inverters as possible to improve the efficiency and thus increase the BESS profitability [17, 33]. The literature still offers only very little PDA investigation in combination with testing in field applications.

2.2 Battery efficiency

The battery efficiency is dependent on various factors. The most important factors are the battery chemistry, the SOC, the C-rate, and the temperature. In BESS, all these factors can be influenced. While the battery chemistry cannot be changed after the investment, the SOC and C-rate can be influenced by the EMS and a PDA.

In Table 1, different efficiency values for BESS from the literature are listed. Those meet the measured efficiency values from M5BAT given in Table 2.

Table 1: Technology-specific battery efficiency for battery storage systems

Technology	**Ah-Efficiency in %**	**reference**	**kWh-Efficiency in %**	**reference**
PbA[2]	90-98	[34, 35]	70-90	[34, 35]
LMO-C[3]	99	[36]	98.4; 96	[37]
LFP-C[4]	98	[36]	96.3; 94	[37, 38]
NMC-C[5]	98	[36]	98.4; 96	[37, 38]
NCO-LTO[6] (NCA-C[7] & LFP-LTO[8])	95	[36]		
LTO[9]			95-99	[39]

The battery efficiency's dependence on the SOC is presented in Figure 1. The efficiency of LFP and NMC batteries is comparatively low in the lowest SOC region [40, 41]. For LFP batteries also, the uppermost %-points show a reduced efficiency [40, 41]. For the operation

[2] Lead-Acid battery; Values for photovoltaic-systems and hybrid electric vehicle batteries

[3] Lithium manganese oxide cathode and graphite anode

[4] Lithium iron phosphate cathode and graphite anode

[5] Lithium nickel manganese cobalt oxide cathode and graphite anode

[6] Lithium cobalt oxide cathode and lithium titanate oxide anode

[7] Lithium nickel cobalt aluminium cathode and graphite anode

[8] Lithium iron phosphate cathode and lithium titanate oxide anode

[9] Lithium titanate oxide anode

of those batteries in a BESS, this means the lowest and highest SOC region should be avoided to keep the efficiency as high as possible.

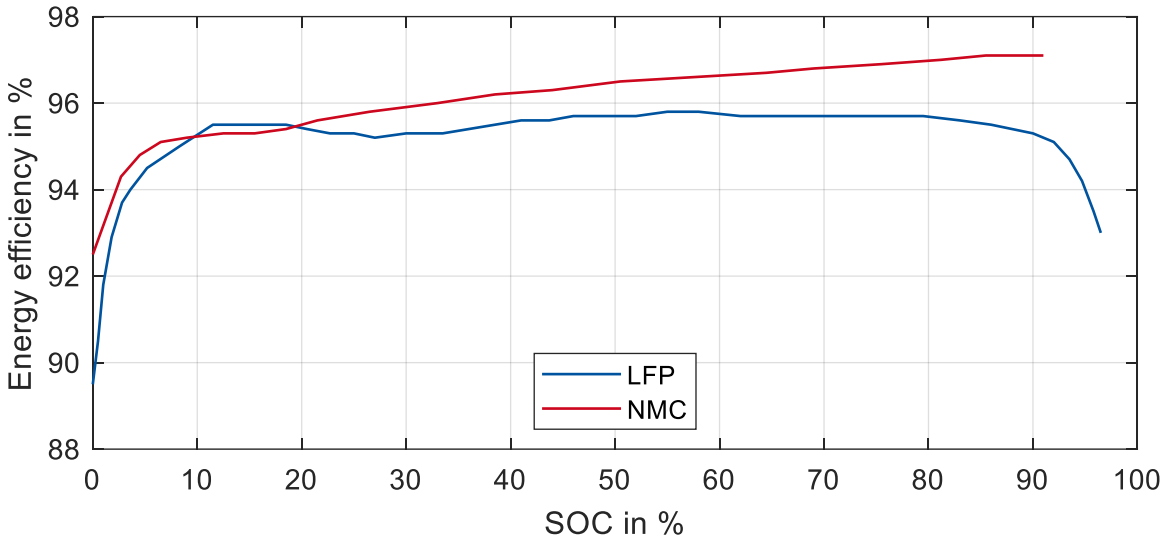

Figure 1: Battery efficiency per battery chemistry over SOC according to [40]

In the case of lead-acid batteries, the efficiency at high SOC states is dramatically reduced, according to Stevens and Corey [34]. The efficiency also decreases with increasing C-rate for lead-acid batteries [35]. This effect also occurs with lithium-ion batteries, although less pronounced [38, 39, 41].

2.3 Battery aging

Battery aging is a significant factor in the economic evaluation of BESS. If the aging of the batteries is lower than assumed at the time of investment, and thus the lifetime of the BESS is longer than expected, further profit can be generated with the BESS. Especially regarding grid services, the calendar aging caused by increased temperature and the cyclic aging cause by high C-rates are the main aging factors [42]. However, the BESS application also affects battery aging. For example, frequency regulation power leads to less aging than energy arbitrage trading [38]. Due to the limited availability of field data on battery aging in BESS, digital twins and simulations are utilized to create an aging path for BESS based on cell data, as demonstrated by Reniers and Howey [43]. In the following, the calendar aging concerning the SOC is summarized from the literature. In Figure 2, the capacity loss per year over the SOC is presented. Since the end of life is typically defined at a remaining capacity of 80%, this means a service life of 20 years at a simplified calendar linear aging rate of 1%. However, since some manufacturers over-dimension the battery capacity due to warranty regulations, the service life may be longer.

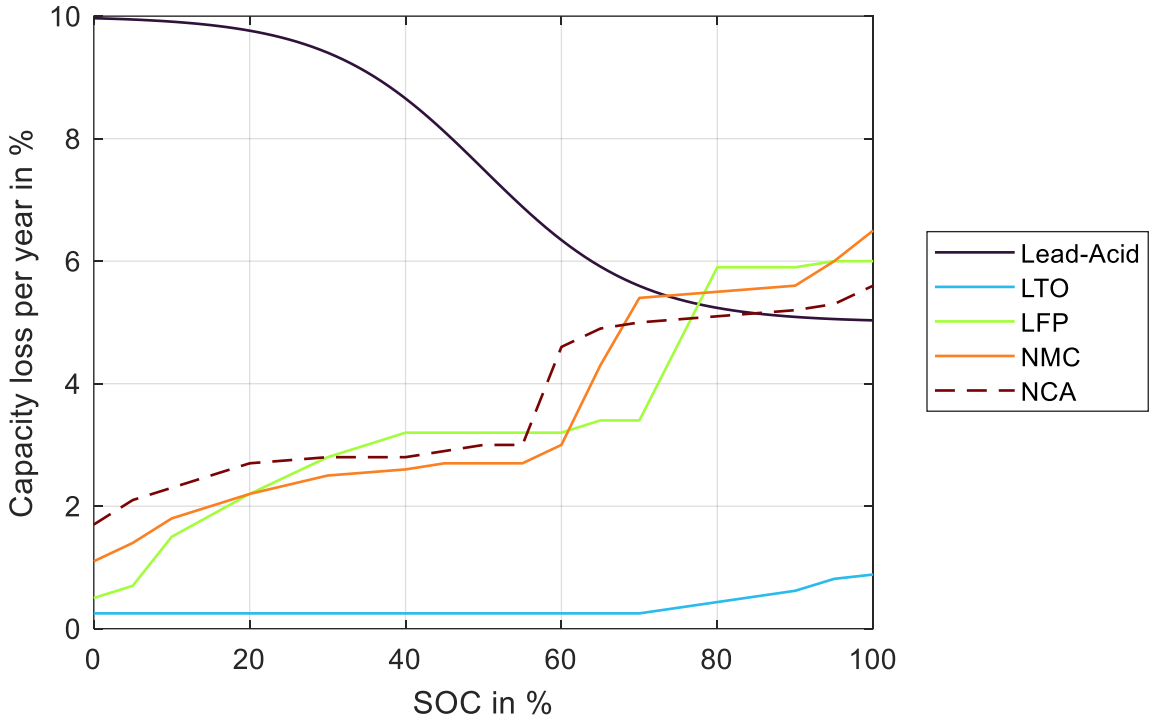

Figure 2: Capacity loss per year for different battery chemistries according to [44–47] calculated to 25°C.

Figure 2 shows that for all lithium batteries, low aging can be expected at low SOCs, and the aging rate increases with increasing SOC. Consequently, to keep the calendar aging low, low SOCs should always be aimed at lithium batteries. While LTO batteries exhibit minimal calendar aging, other battery technologies such as NMC, NCA, and LFP age much faster [44, 46]. Noticeably, there is a sharp increase in the aging rate at 55% SOC for NCA, 60% SOC for NMC, and about 70% SOC for LFP. For more nickel-rich NCA batteries this increase in the aging rate is shifted towards higher SOCs [48]. Keil *et al.* [44] located this increase in aging at the central graphite peak of the tested batteries. Thus, in normal operation, these battery technologies should be operated below these limits if possible. For lead-acid batteries, the opposite aging behavior is known. At high SOCs, these batteries age slower than at low SOCs [47]. However, the aging rates of lead-acid batteries are higher than those of lithium batteries. Thus, high SOCs should be targeted for lead-acid batteries.

3 Battery storage system M5BAT

The modular multi-megawatt medium voltage battery storage system (M5BAT) has been built for testing and evaluation of individual battery performance and hybrid operation. M5BAT has already been investigated in several studies regarding various aspects. The planning and first optimizations were published in [19, 49]. Data evaluations over several years on the impact of ancillary services such as frequency containment reserve were also conducted [20, 50, 51]. The reaction speed and optimizations in reaction time were separately investigated [13]. The EMS development, including the PDA, is continuously improved, as shown in [15, 17, 18]. In comparison to these analyses, this paper focusses on the improvement of functionality and efficiency by the PDA. In the following section, the technical data of M5BAT and the grid service of FCR are explained.

3.1 Technical data

M5BAT consists of ten battery units of five different battery technologies. Each battery unit has an individual inverter, as shown in Figure 3. Two inverters are connected to one transformer, and all five transformers are connected to one grid connection point. The grid connection takes place on the medium voltage level, while the inverters work on 315 V on the AC side and between 500 V and 900 V on the DC side (see Figure 3). The whole system is controlled by an EMS system, and data is logged and stored by an automatic datalogger.

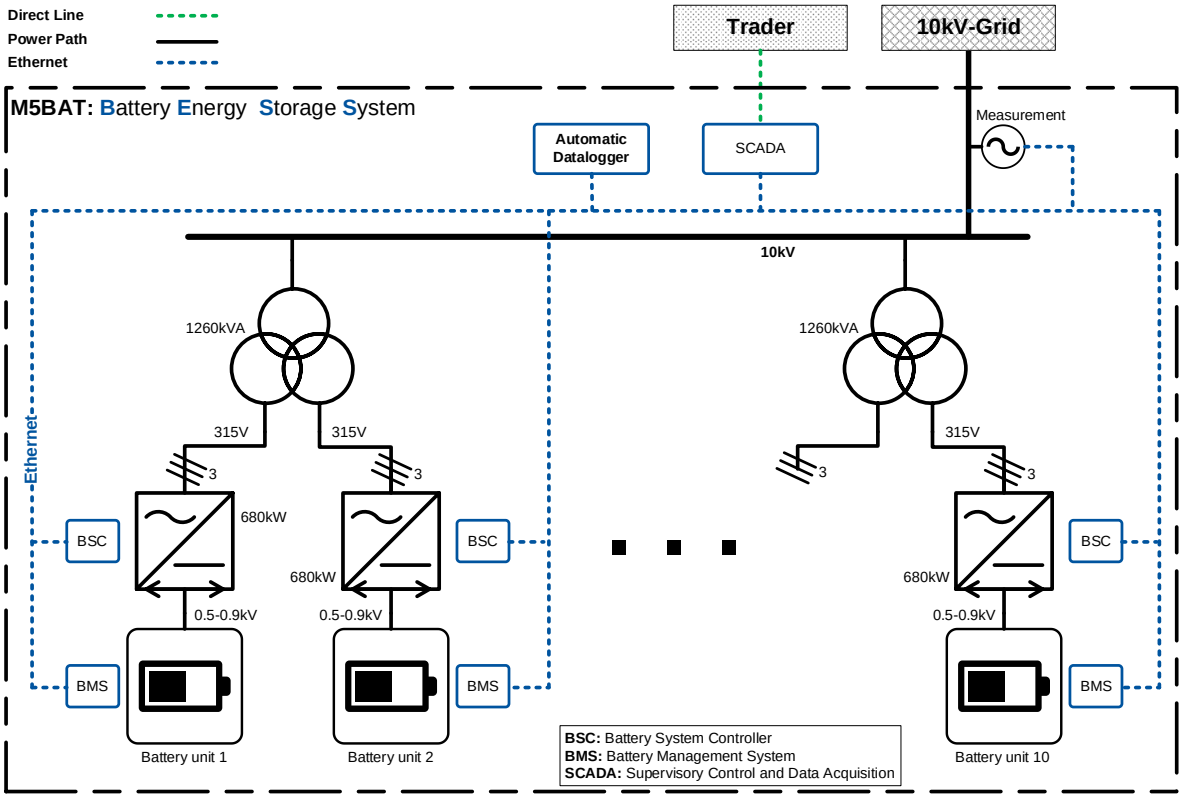

Figure 3: M5BAT connection scheme and structure – status 2023. Adjusted and updated from [16, 18–20, 49]

The ten battery units have different sizes in terms of nominal energy and nominal cycle numbers. Those technical data can be found in Table 2. To get an overview of the battery efficiency and the battery utilization, the average C-rate and efficiency values are also provided for each battery unit for 2022 in Table 2. Performance tests and results for the BESS M5BAT can be found in [52].

Table 2: Technical battery description of the battery units and technologies of M5BAT [20, 50–53]. The shown C-rate takes only data points with an absolute current larger than 0.01 C into account.

Bat-tery unit	Techno-logy	Acro-nym	Short	Nominal energy at 1/3C in kWh	Nominal number of cycles	measured kWh effi-ciency in % in 2022	measured Ah effi-ciency in % in 2022	Measured average C-rate in 2022
1	OCSM[10]	Pb1	P1	1066	1500	83.98	96.88	0.1521
2	OCSM	Pb2	P2	1066	1500	86.63	99.20	0.1586
3	OPzV[11]	Pb3	P3	843	2400	81.88	93.66	0.1452
4	OPzV	Pb4	P4	740	2400	81.93	96.53	0.1618
5	LMO/NMC	LMO1	L1	774	6000	97.82	99.11	0.2374
6	LMO/NMC	LMO2	L2	774	6000	97.93	98.22	0.2368
7	LMO/NMC	LMO3	L3	774	6000	98.06	98.35	0.2368
8	LMO/NMC	LMO4	L4	774	6000	97.79	99.08	0.2401
9	LFP	LFP	L5	738 (923)	5000	96.36	99.00	0.2323
10	LTO	LTO	L6	230	>12000	95.95	100.25	0.5312

3.2 Frequency containment reserve

Ancillary services are used to keep electricity grids stable. In the European interconnected grid, several types of control reserves with different reaction speeds are implemented [54]. The FCR service requires the quickest response times in Germany and is, for most assets, the most challenging service [55, 56]. The FCR provision follows a specific droop curve dependent on the frequency deviation and defined by the transmission system operators [56, 57]. Within this curve, degrees of freedom, such as the use of the deadband or 20 % overfulfillment, are allowed, bringing flexibility to battery operation [56–58]. Since BESS can react very fast, they easily meet the requirement for FCR and are well suited for this service [55].

The deadband is in the frequency range of $\pm 10 mHz$ around the target grid frequency of 50 Hz. Within the deadband, no action is required, but it can still be provided. In the case of BESS, 100 % of the offered FCR power has to be delivered at 50.2 Hz in the charging direction, while at 49.8 Hz, 100 % of the provided FCR power has to be discharged [56–58]. The droop curve must be followed between those boundaries with automatic activation.

[10] Lead acid battery with liquid electrolyte

[11] Lead acid battery with gelled electrolyte

4 Methodology

The methodology is divided into a section about the improved version of the PDA, the efficiency description of the power conversion system, and the performed testing procedures.

4.1 Modular staged-rule-based power distribution algorithm V.2023

The staged rule-based power distribution algorithm in version 2023 increases the efficiency of the large-scale BESS M5BAT. It reaches a predefined energy throughput share while keeping the already achieved advantages of the SPDA V.2022. The SPDA V.2022 is designed to use the battery units in a way that power output, efficiency, and aging are optimized [17]. To the existing four prioritization levels, a fifth level was set on top only to distribute small power requests and prevent frequent switching of the inverters. In Figure 4, the new stack of prioritization stages is shown.

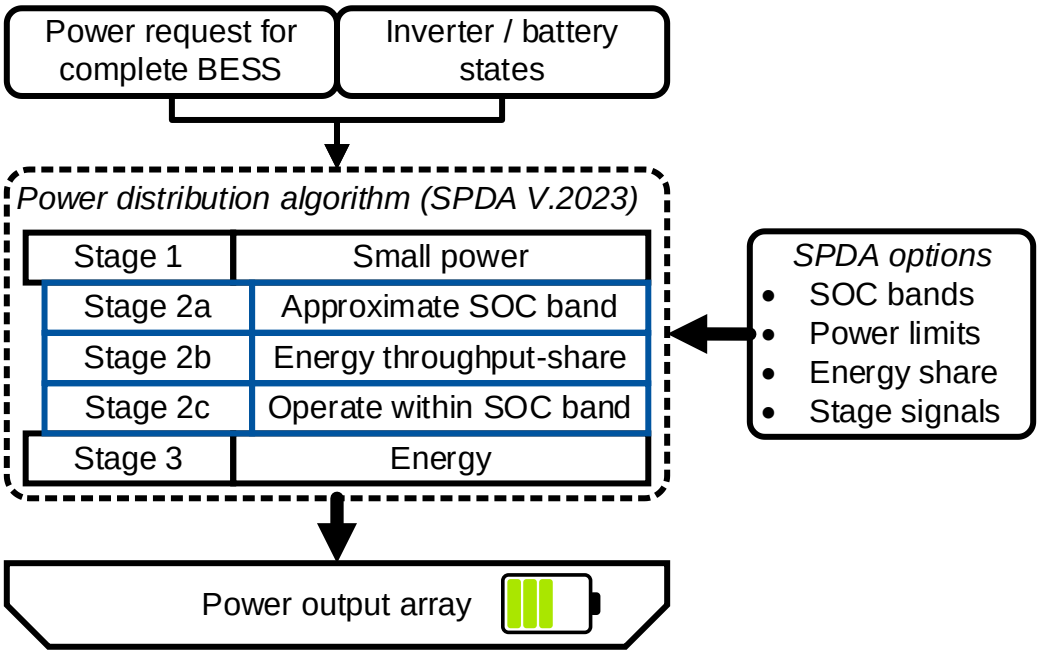

Figure 4: Schematic stack of stages of the SPDA V.2023, including the relevant inputs, outputs and options.

Next to the new prioritization level, the efficiency-optimizing options listed in Table 3 were introduced. The corresponding objectives can also be found in Table 3.

Table 3: Efficiency-optimizing options and their objectives

Efficiency-optimizing options	Objective
Inverter non-use power if stage boundaries are not reached	Power outputs smaller than the inverter non-use power should be reduced
New inverter threshold and hysteresis power	Improved inverter efficiency
Option to prefer battery units connected to the same transformer	Increase of the transformer utilization
Controller threshold power	Fewer controller actions caused by the inaccuracy of measurement
Pre-control transformer losses calculation	Minimize the controller actions
Pre-control reactive power calculation	Minimize the controller actions

Next to the optimization, the SPDA V.2023 stays ready and compatible for value-stacking and multi-use operation. Since the SPDA V.2023 is always optimized according to the power distribution rules, the input power request is the only relevant parameter. Especially for partial loads, the SPDA V.2023 can gain significant advantages.

In the following section, the changes from the SPDA V.2022 to the SPDA V.2023 are explained in detail. The stages or levels of the SPDA V.2022, which are identical to the SPDA V.2023, are only briefly repeated. The flowchart in Figure 5 shows the complete process of all stages of the SPDA V.2023.

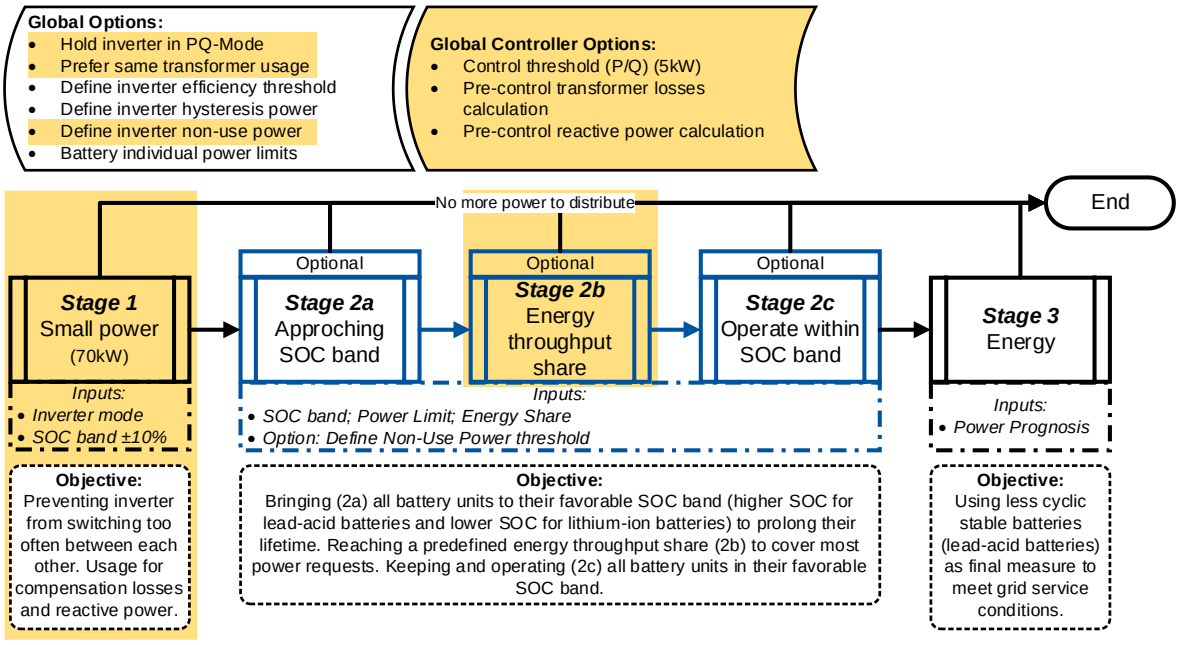

Figure 5: Flowchart of the SPDA V.2023 including all stage objectives and stage inputs as well as global options for the SPDA V.2023 (see also [17]). All new developments in the SPDA V.2023 compared to the SPDA V.2022 are marked in orange.

4.1.1 Stage 1: Small power prioritization

The new prioritization stage 1 for small power requests has two globally valid user input options. The first option is the maximum power value, while the second is the enlargement of the individual SOC bands. As in Figure 5, the maximum power value is set to 70 kW, which means that stage 1 is only active if the input power request for the whole BESS is lower than 70 kW charging or discharging power. If a larger power request is given to the SPDA V.2023, stage 1 will not distribute any power but will forward the power request to the next stage to handle it. The expansion of the SOC bands is a percentage which is added to the individual SOC bands from stage 2a/b/c. The enlarged SOC bands are only valid for stage 1 and are not changed for stage 2a/b/c. The expansion is made to prevent frequent inverter changes if the SOC levels are close to or at the boundaries of stage 2a/b/c.

In stage 1, the small power request often appears in real-world conditions if no power is requested by grid services such as FCR, but the transformer and inverter losses have to be compensated. Usually, this compensation is a small power request in discharging direction for the battery units. In stage 1, only one battery unit can be chosen and the battery unit which was active in the last calculation period and is within its enlarged SOC band is chosen. If multiple battery units were active in the last calculation period, the battery unit with the highest order number, according to Table 2, is chosen. These rules cause the last active battery unit to keep active until a larger power request to the BESS is made. Frequent changes of active inverters are reduced, which increases the reaction speed and efficiency. The inverter mode change between standby and active mode takes around 2 s and does not occur if the already active inverter is used [13]. A fictive example in Figure 6 shows the change in the behavior between the SPDA V.2023 and the SPDA V.2022 [17].

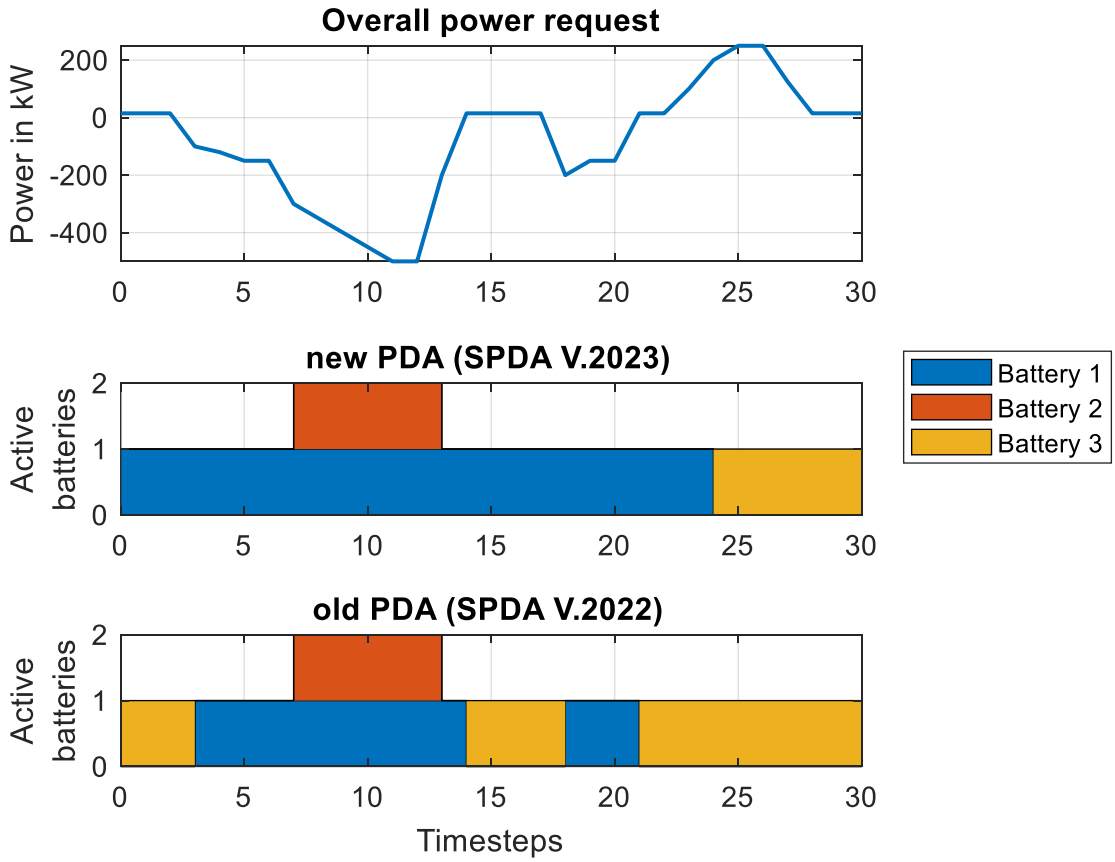

Figure 6: Switching behavior comparison between SPDA V.2022 and SPDA V.2023 [59]

In the top graph of Figure 6, a fictive power request profile is shown. Included are sections of low power demand intended to show idle operation or loss compensation, and sections of higher charge and discharge power requests intended to show FCR operation. In the middle graph, the activation of battery units with the SPDA V.2023 is shown, while the lower graph shows the battery unit activation with the SPDA V.2022. In the idle sections, the SPDA V.2022 makes a switchover if the battery unit was previously charged. Stage 1 of the SPDA V.2023 delays this switching process, or only carries it out when changing from a charging phase to a discharging phase with a higher power. The reduction of the switching processes thus leads to longer utilization and phase phases of the individual battery units.

4.1.2 Stage 2a: Approaching the SOC band

This optional stage 2a has remained unchanged since the last iteration of the SPDA (SPDA V.2022). The stage is described in [17]. For the prioritization stages 2a, 2b, and 2c, a common SOC band is defined for each battery unit. In stage 2a, the distance to the specified SOC band is used as a sorting variable. The sorting algorithm has a hysteresis of 5 % implemented to prevent frequent switching between battery units. The battery unit can be charged if the target SOC band is undercut, while a discharge is possible when the SOC band is exceeded.

4.1.3 Stage 2b: Energy throughput balancing

For the optional stage 2b, the SOC bands are shrunk by 5 %. In this SOC band, the energy throughput should be leveled out to a predefined share per battery unit. Any charging or discharging of the battery unit, independently of the stage, is counted as energy throughput according to formula (1).

$$E_{thru} = E_{cha} + E_{dis} \tag{1}$$

The energy throughput balancing is executed in iterations of equivalent energy throughput. Both, the energy throughput of the entire BESS and the target energy throughput of the individual battery units are relevant here. The balancing iterations are visualized in Figure 7.

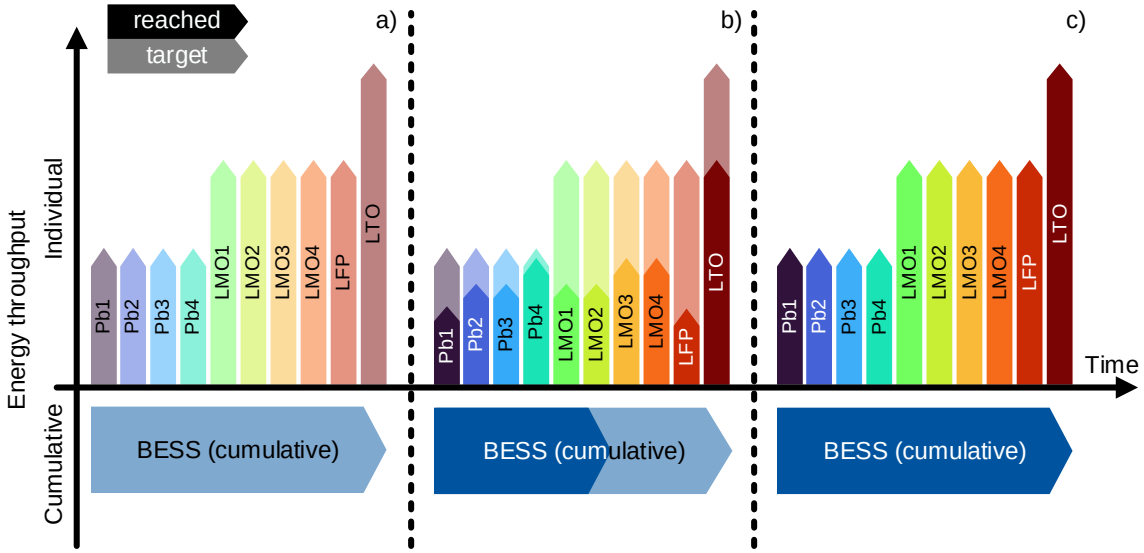

Figure 7: Schematic visualization of the energy throughput balancing for one iteration.

The energy throughput balancing is achieved once a defined cumulative energy throughput of all battery units has been reached (Figure 7 c)). For each battery unit, the targeted energy throughput in kWh is set by the user. The cumulative energy throughput is the sum of all battery units' targeted energy throughput. The maximum cumulative energy throughput is currently set to about 32,767 kWh, which is based on the use of 16-bit integer variables. After the cumulative energy throughput is reached, the process of energy throughput balancing is started again. Within the process, each battery unit has an energy counter which counts downwards to zero indicating the remaining energy throughput until the defined share is reached. The sorting algorithm uses the remaining energy counter as a sorting variable.

If some battery units must be operated to fulfill the grid service or currently driven application but the remaining energy throughput of this battery is already zero, a second remaining energy counter is activated. The second energy counter indicates the next iteration of the energy throughput balancing. If one cycle of energy throughput balancing is finished, the second battery unit energy counter is moved to the first counter, and the first counter is

reset. In this way, the energy throughput balancing is also possible over a longer period of time, including the balancing of edge cases of battery unit operation to fulfill grid services with already reached energy balancing targets.

Related to Figure 7 a), no energy throughput is achieved, and the process starts. In Figure 7 b) all batteries already reached a portion of the energy throughput, but some batteries are closer to their goal than others. The difference between the targeted energy throughputs and already reached energy throughputs is the largest for the LFP battery unit followed by all other lithium-ion battery units. Hence, the LFP battery unit is preferred for the next requested energy throughput. If all battery units reached their targeted energy throughput the balancing iteration in Figure 7 c) is finished and the cumulative energy throughput counter is reset for the next iteration.

Furthermore, this stage can only distribute a maximum power that the user can set to each battery unit. The maximum power value should be set to a value where the PCS operates most efficiently. This setting helps to reach high efficiencies.

The stage eliminates the energy throughput dependence on the size of the SOC bands.

4.1.4 Stage 2c: Operating within SOC band

The prioritization stage 2c was the previous stage 2b [17]. When the energy throughput balancing stage 2b is activated, it is assumed that this stage is used less frequently than before. Suppose the remaining power is passed on to stage 2c after the previous stages. In that case, the battery units' distances to the SOC band limits are calculated as sorting variables, considering a 5 % hysteresis margin. Battery units with a considerable distance to their SOC limits get an additional power request to the previously distributed power. This helps to reach the SOC limits of all battery units as evenly as possible.

If there is still power left to distribute after stage 2, the remaining power will pass on to the last stage of the algorithm.

4.1.5 Stage 3: Energetic prioritization

Stage 3 of the SPDA V.2023 remains unchanged from the previous iteration [17]. This stage is always active, and the battery units are sorted according to the available charging or discharging energy. The battery units with the largest power forecast are thus preferred. The quality of the stage remains dependent on the accuracy of the power forecast of the BMS of the battery units [17].

4.1.6 Global efficiency options

Next to the presented stage 1, global options are added to the SPDA to create the SPDA V.2023. For stage 2a/b/c, an inverter non-use power option is defined. The user can customize this option and prohibits those stages from using a battery unit if the instant power prognosis is lower than the non-use power option. If the battery unit is approaching or within

the defined SOC band and the power output is very small, the battery unit cannot be used. This behavior appears from time to time in real-world BESS. By preventing those small power outputs, the inverter efficiency is not affected greatly, and the overall efficiency can be increased.

The inverter efficiency threshold and inverter hysteresis power are further developed to user input values. This allows for optimization and in-operation adjustments. Furthermore, an option to prefer battery units connected to the same transformer is integrated. This increases the utilization of the active transformer while the other transformers are not used. If this option can increase the efficiency significantly will be determined within this study.

Due to the results of the reaction speed study [13], an option to keep the inverter in power output mode or active mode was integrated. The option can be used for faster grid services where a switching time of more than 1 s is too slow.

Next to those options, the global controller for the active and reactive power at the grid node was updated. A user-configurable controller threshold value is integrated. It can set a certain band around the target value where the controller needs to work. Noise on signals and measurement uncertainties make this option useful. Also, pre-controller transformer losses and reactive power calculations are integrated. Both pre-controller functions give an estimation to the controller. The controller itself now has fewer steps to compensate and needs just to do a fine adjustment. In which manner those options affect efficiency is not yet known.

4.2 Efficiency of the power conversion system

The efficiency of the power conversion system (PCS), which in the case of M5BAT consists of converters and transformers, strongly depends on the chosen operating point. For each component, there is a specific optimal efficiency operating point. From this analysis of the optimal operating points, general rules for the global efficiency options can be derived.

4.2.1 Components: Transformer and inverter

In terms of efficiency, there is an optimal operating point for transformers. However, regarding the utilization of transformers at different operating points, it can be stated that if the losses are kept as low as possible, the efficiency will be as high as possible.

Five identical transformers are used in M5BAT. Iron losses always occur because the transformers cannot be switched off during operation, and copper losses depend on the transformer current and, thus, on the power converted. In Figure 8, the resulting losses in different scenarios are shown. If the power is distributed evenly throughout all transformers, the losses are the lowest. On the other hand, if all transformers are activated in sequence one after each other, the highest losses occur.

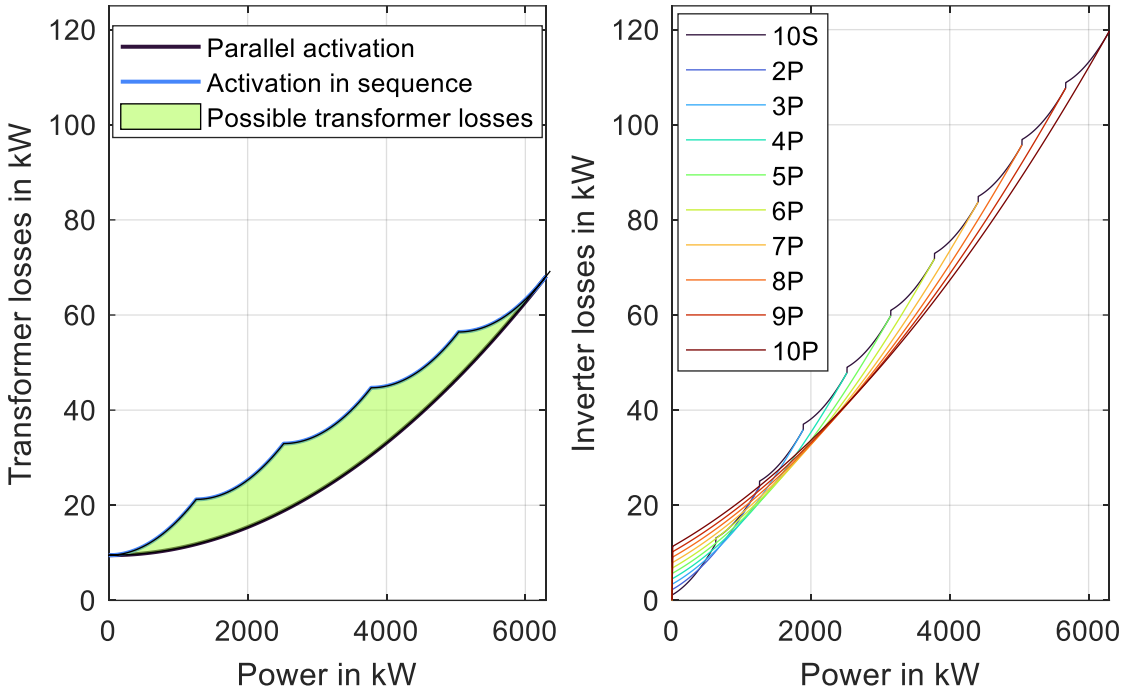

Figure 8: Left: M5BAT transformer losses curves for best- and worst-case scenarios [60]. Right: Inverter losses curves for parallel (P) and series (S) activation [61, 62]. The efficiency curves and resulting losses curves were modeled with the approach from Sauer and Schmidt [63].

According to Figure 8, the losses will always be in the green-marked zone, and the target is to come as close to the lower boundary as possible.

In contrast to the transformers, all inverters can be put into standby mode where no losses occur except for the auxiliary supply. In M5BAT, ten individual inverters are used. Figure 8 shows the inverter loss curves for different activation sequences. It was assumed that the power was distributed equally among all activated converters. It becomes clear that there is an optimal number of activated inverters for each power request.

For a power request lower than 400 kW, only one inverter should be used. From then on, nearly every 284 kW, another inverter should be activated. With the global efficiency options, especially the efficiency threshold power and the inverter hysteresis power, activation of the inverters close to the optimal version from Figure 8 can be achieved.

4.2.2 Power conversion system

For the PCS, the effects of the transformers and inverters overlap, and an optimal number of used inverters and transformers results for each power request. For the assumption that the power is always evenly distributed, the power loss curves result from Figure 16. The behavior seen from the inverters continues, but the optimal number of activated inverters shifts on the power axis. All other combinations of the activation sequence will result in a

loss curve that lies in between the shown curves. The combination of inverters and transformers leads to discrete power levels when to use how many inverters and transformers. These power levels from Figure 16 are listed in Table 4.

Table 4: Efficiency optimal power ranges for a certain number of activated inverters and transformers

Active inverters	Active transformers	Power in kW	Min. inverter power in kW	Max. inverter power in kW	Difference in kW
1	1	0 <= 325	0	325	325
2	2	325 <= 562	163	281	237
3	3	562 <= 794	187.7	264.7	232
4	4	794 <= 1024	198.8	256	230
5	5	1024 <= 1549	205	309.8	525
6	5	1549 <= 1833	258.3	305.5	284
7	5	1833 <= 2116	262	302.3	283
8	5	2116 <= 2400	264.6	300	284
9	5	2400 <= 2683	266.8	298.1	283
10	5	> 2683	>268.3		
BESS (Mean)	-	-	207.42	263.6	284

Table 4 suggests using the different transformers as quickly as possible. Each time an additional inverter is activated, it is best to activate an inverter connected to a different transformer. On average, another inverter should be activated every 284 kW, resulting in an average minimum power of 207 kW and an average maximum power of 264 kW until all inverters are activated.

If the global efficiency options are introduced as efficiency threshold power, and the inverter hysteresis power should be used, the exact values cannot be met. But with the following approach, an approximation can be made.

The efficiency threshold power ($Hysteresis_{lower}$) and the inverter hysteresis power ($Hysteresis_{upper}$) add up to 284 kW, which means that every 284 kW a new inverter is activated.

$$284\ kW = Hysteresis_{upper} + Hysteresis_{lower} \quad (1)$$

Also, the efficiency threshold power must be smaller than half the inverter hysteresis power.

$$Hysteresis_{lower} < \frac{Hysteresis_{upper}}{2} \quad (2)$$

Additionally, a minimum inverter efficiency marks the lower boundary for the efficiency threshold power. Since with a minimum efficiency of 98 % no more solutions are available, the lower limit of the power is rounded to 70 kW.

$$Hysteresis_{lower} > 72kW\ (97{,}5\%\ \eta_{inverter})$$
$$Hysteresis_{lower} > 112kW\ (98\%\ \eta_{inverter}) \quad (3)$$

This defined problem allows solutions for the efficiency threshold power and inverter hysteresis power between 70 to 215 kW and 95 to 190 kW. The two named boundary solutions will be tested and are thus listed in Table 6.

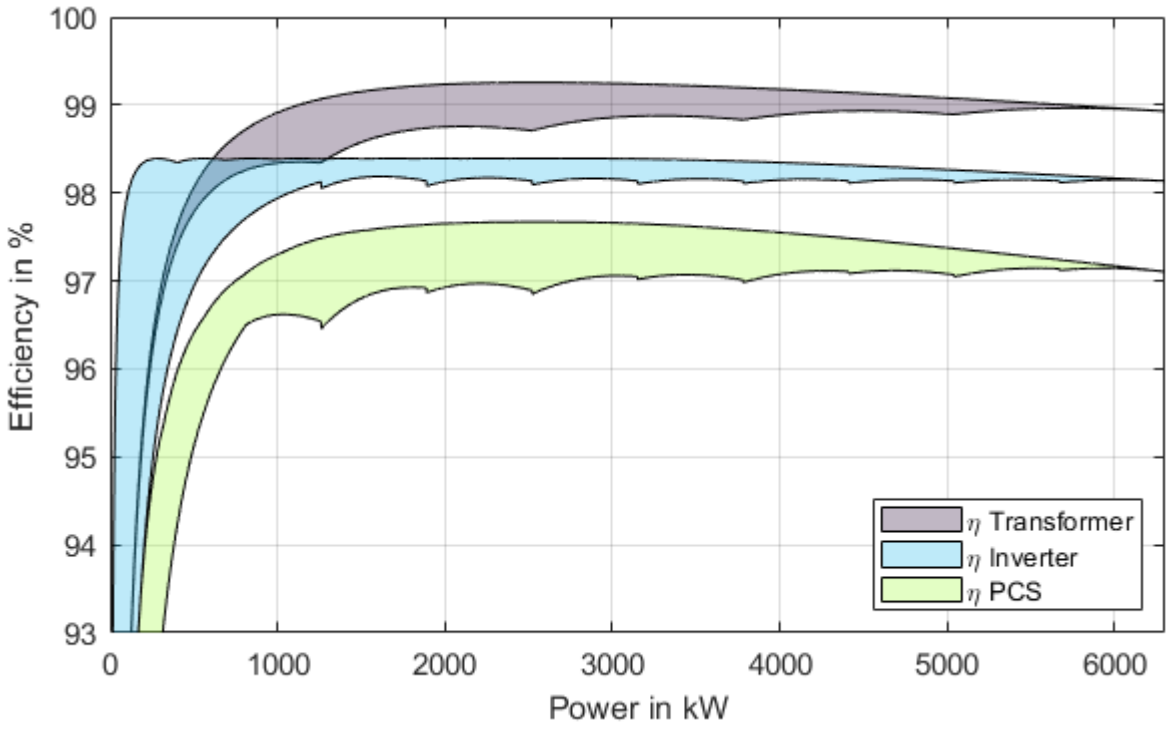

Figure 9: Efficiency areas for the transformers, inverters, and the PCS of M5BAT.

4.3 Testing procedures after all improvements

The testing procedures are made in four independent testing sessions. Each test was performed for the duration of one week with all battery units available. Test X, according to Table 6, is a fifth test that just includes a full cycle of two LMO battery units. This test serves as a benchmark for the maximum achievable efficiency. The shown power distribution rules in Table 5 were valid for all testing procedures, except for Test X.

Table 5: Power distribution settings valid for all performed tests.

Test	**Battery unit ►** / **Level of prioritization ▼**	**1 – 4**	**5 – 8**	**9**	**10**
STD	Level 1	SOC Level 2 ±10 %			
	Level 2 a,b,c	45-70 %	25-60 %	35-70 %	30-70 %

	Level 3	For all battery units on

In Table 6, the inverter hysteresis power, as well as the stage 1 power and stage 2b usage, are shown. The targeted energy share for test sessions 1 and 2 are presented in Table 7.

Table 6: Test names and chosen settings for the tests.

Test	**Use batteries on same transformer**	**Inverter hysteresis power**	**Non-Use & stage 1 power**	**Stage 2b**	**Prioritizations used**
X		Full load cycle		Not relevant	
1	No	70-215 kW	70 kW	Yes	STD
2	No	70-215 kW	70 kW	Yes	
3	No	70-215 kW	70 kW	No	
4	No	95–190 kW	95 kW	No	

Table 7: Targeted energy share per battery unit.

Battery	Energy (Test 1) in %	Energy (Test 2) in %	Energy (Test 1) in kWh	Energy (Test 2) in kWh
1	5	5	500	500
2	5	5	500	500
3	2.5	2.5	250	250
4	2.5	12	250	1200
5	12	25	1200	2500
6	12	12	1200	1200
7	12	12	1200	1200
8	12	12	1200	1200
9	12	12	1200	1200
10	25	2.5	2500	250
BESS (Sum)	100	100	10,000	10,000

The energy throughput balancing should be achieved each 10,000 kWh. If the achieved overall energy throughput exceeds 10,000 kWh by multiple times, the error in terms of difference from the target is reduced. The different settings chosen in Test 1 and Test 2 should show that stage 2b can reach the targeted energy throughput balance independent of the SOC band sizes.

5 Results

The test results of the improved power distribution algorithm are reported as follows. First, the functionality of the newly integrated stages and the effects of those are reported. Afterwards, the benchmark test under full load is presented. Then, the efficiencies of all components are analyzed individually, and finally, the resulting system efficiency is shown.

5.1 SPDA V.2023 functionality

The SPDA V.2023 functionality results are divided into investigations that verify the operability of the different stages of the SPDA V.2023. The small power stage 1 is investigated by the inverter switching behavior in section 5.1.1. Following, stages 2a and 2c are examined by the battery SOC distribution in section 5.1.2. The energy throughput balancing stage 2b is shown in section 5.1.3 with the energy shares.

5.1.1 Inverter switching behavior

The aim of stage 1 is the prevention of frequent inverter changes to get more constant use and avoid delay times due to inverter switching. In Figure 10, the number of inverter activations per week is shown. The activation is switching from standby to power output mode. As a comparison to the tests performed in this study, the mean values for 2021, 2022 and the previous generation of the SPDA are given.

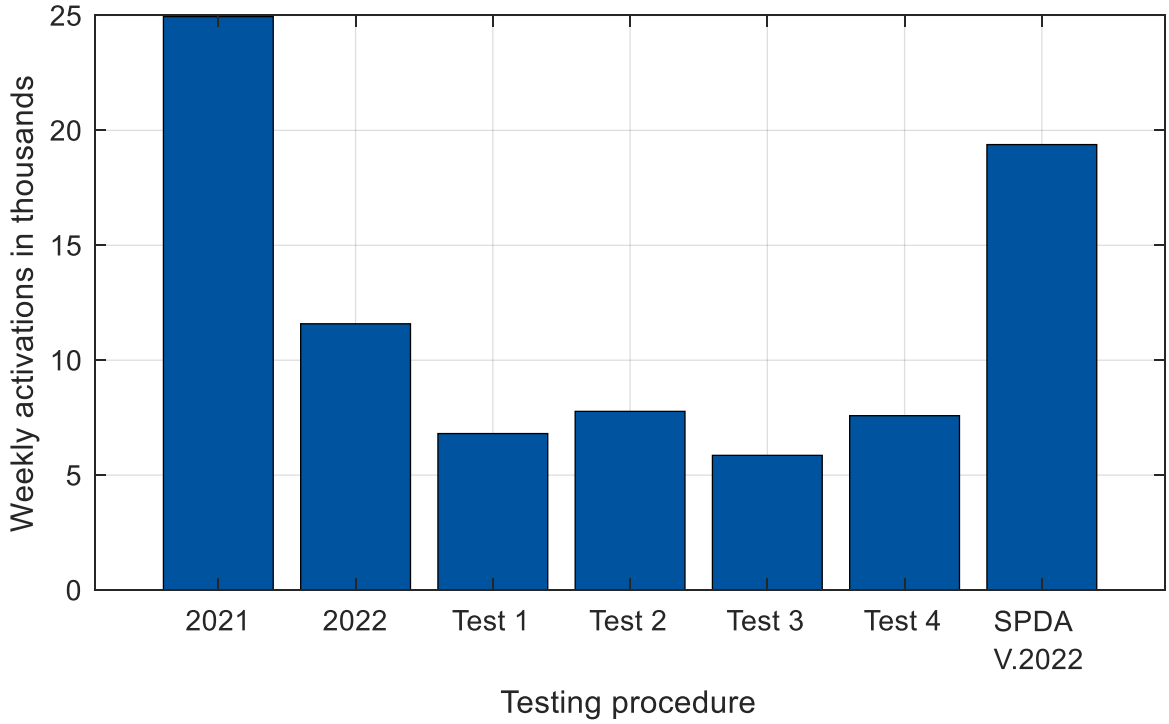

Figure 10: Number of inverter activations (switching from standby to power output mode) per week.

The inverter activations per week in Figure 10 reveals a reduction in inverter activations from 25,000 in 2021 to around 6,000 in the recent tests, which is a reduction of approximately 75 %. Due to the implementation of stage 1 of the SPDA V.2023 in late 2022, the mean value in 2022 is reduced to ~11,500 activations per week and thus significantly lower than in 2021. Comparing the average value of test 1 to test 4 to the average value of the SPDA V.2022 tests, the previous generation of the PDA, the number of inverter activations per week was reduced by 63.8 % [17]. It can be summarized that the goal of reduced inverter activations was achieved by stage 1 and is an improvement of the SPDA V.2023 compared to the SPDA V.2022.

5.1.2 SOC bands

Since the functionality of the SOC band prioritization has remained unchanged compared to the older SPDA V.2022, it is expected to see the maintained SOC bands [17]. The observed SOC distribution for all tests is presented in Figure 11. The aimed SOC bands are marked with red lines with triangles. The boxes indicate 50 % of the values, while the whiskers in each direction indicate the $\pm 2.7\sigma$ boundary.

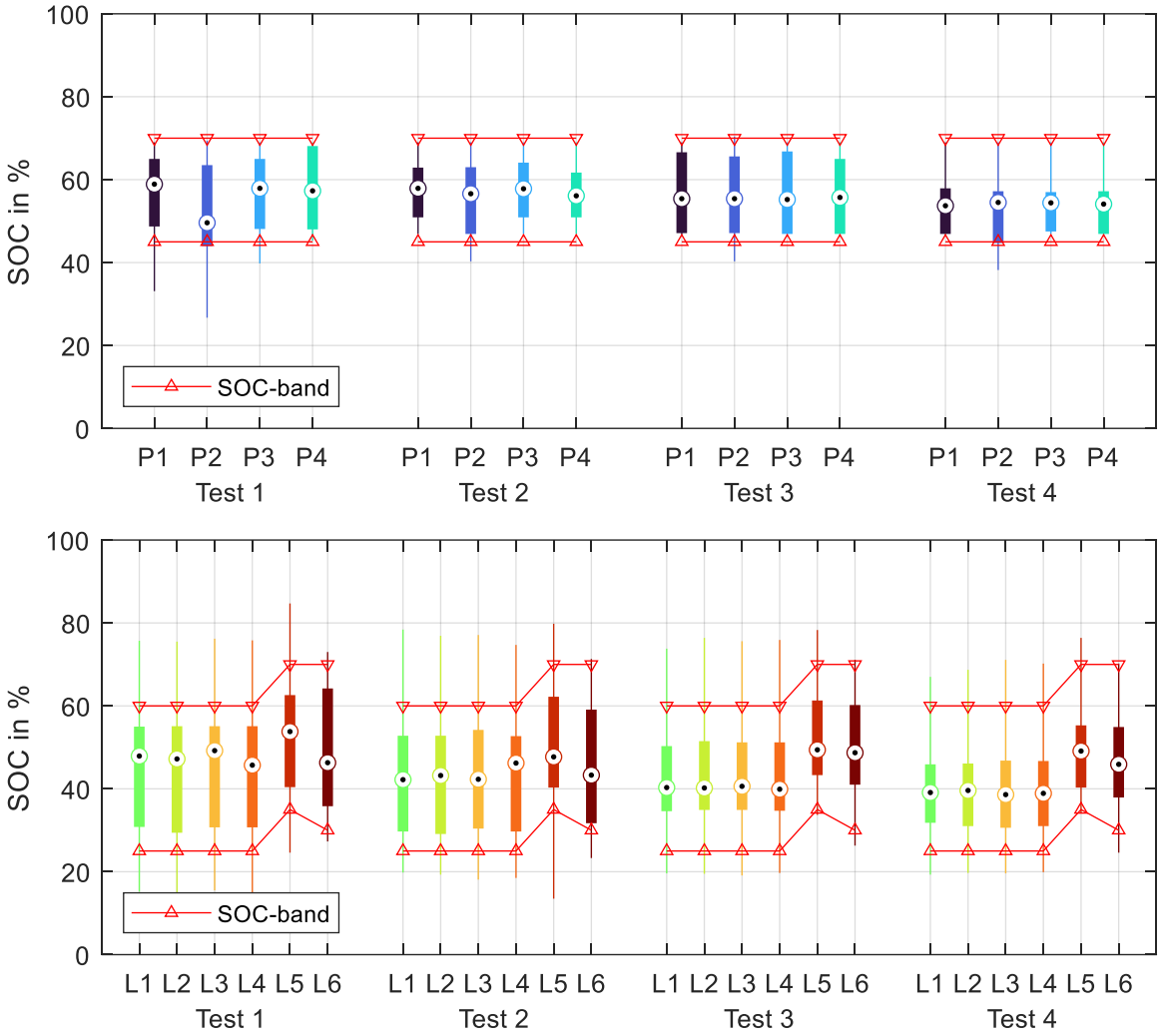

Figure 11: Boxplots of the SOC distribution for each battery unit of M5BAT. The upper subplot shows the lead-acid batteries, while the lower subplot shows the lithium-ion batteries with the shortened acronyms according to Table 2. The red lines indicate the set SOC bands for level 2 according to Table 5 [64].

The majority of all values can be found within the set SOC bands, which confirms the functionality of stages 2a and 2c. The whiskers of the boxplots outside the SOC bands show that there is still the possibility of deviating from the SOC bands due to the advanced delivery of grid services. For these cases, mainly lithium-ion batteries are used. With lead-acid batteries, on the other hand, there are almost no deviations from the desired SOC bands.

5.1.3 Energy share

The energy distributions in Figure 12 are used to evaluate the effectiveness of stage 2b. Stage 2b was only used in tests 1 and 2, while in tests 3 and 4, stage 2b was switched off. The targeted energy throughput shares according to Table 7 are marked with a lowered “T” in Figure 12, while the measured energy throughputs are marked with a lowered “M”. The energy distribution in tests 3 and 4 is thus mainly dependent on the selected SOC bands of

the respective battery units and the nominal capacities or nominal energies of the battery units. Larger SOC bands lead directly to higher energy throughputs, which becomes clear in the case of the LTO battery unit. Despite a lower capacity, the LTO battery unit experiences the highest energy throughput.

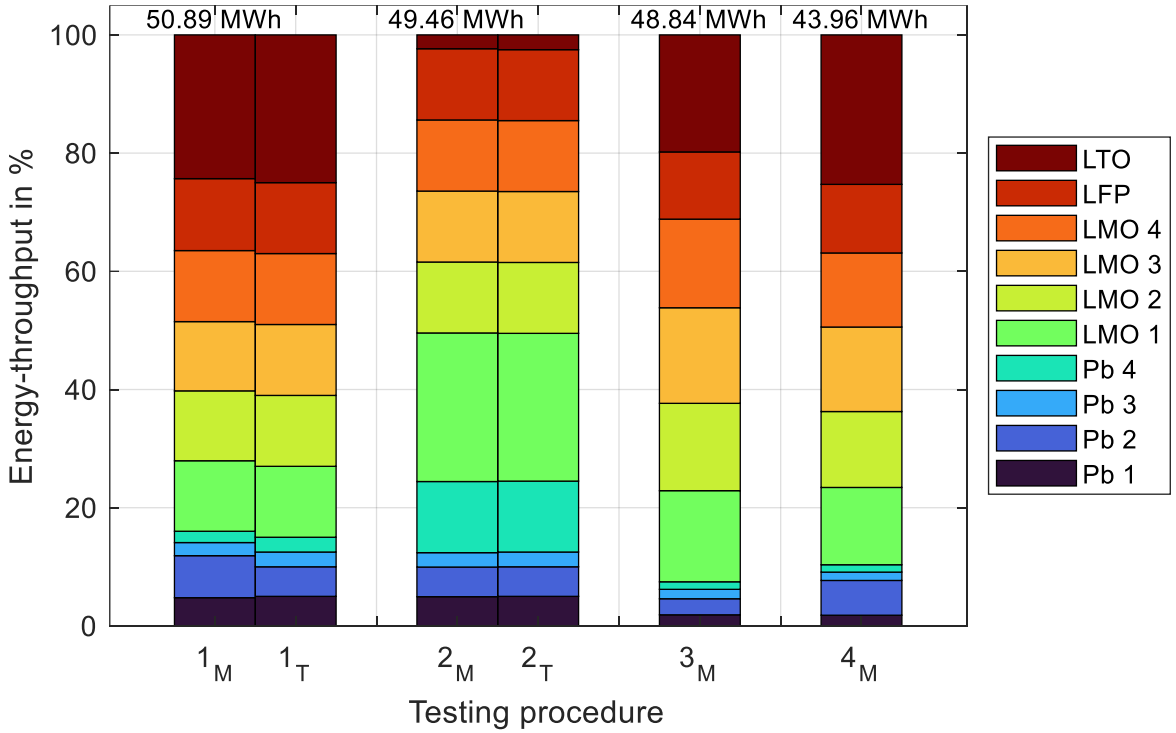

Figure 12: Relative share of energy throughput and absolute energy throughput value for each test. In test 1 and test 2 the lowered M indicates the measured values while the T indicates the target values for the energy throughput.

In tests 1 and 2, the SOC bands were not changed, and yet the energy throughputs are significantly different from tests 3 and 4. Between tests 1 and 2, a ring swap in energy throughputs is visible for the LTO, LMO1, and Pb4 battery units. According to Table 7, this was exactly the planned energy shift. Thus, the pre-planned option of the energy distribution of stage 2b becomes clear, and the effectiveness is confirmed. The energy throughput of the SPDA V.2022 was dependent on the sizes of the SOC bands or the use of the stage for the cyclically stable battery units, as can also be seen in test 3 and test 4. The SPDA V.2023 overcomes this dependency and can eliminate the stage for the cyclically stable battery units. Another advantage of the SPDA V.2023 over the SPDA V.2022 is that the energy throughput can be planned, whereas with the SPDA V.2022 the energy distribution had to be estimated in advance based on operating knowledge.

5.1.4 Power levels

The power distribution is shown exemplary for test 1, while figures and details for all other tests can be found in the appendix. For test 1 the distribution of the BESS power requests is shown on the left in Figure 13. The blue lines mark the inverter hysteresis power setting, while the red lines mark the stage 1 power setting. Theoretically, all power requests within

the blue lines could be fulfilled by just one battery unit, while alle power requests within the red lines must be fulfilled by a single battery unit. On the right side in Figure 13 the distribution of active inverters for power requests between the blue lines or for an absolute power request of $P_{abs} \leq 285\ kW$ is shown. More than 75% of the power requirements are covered by one inverter and just over 20% by two inverters.

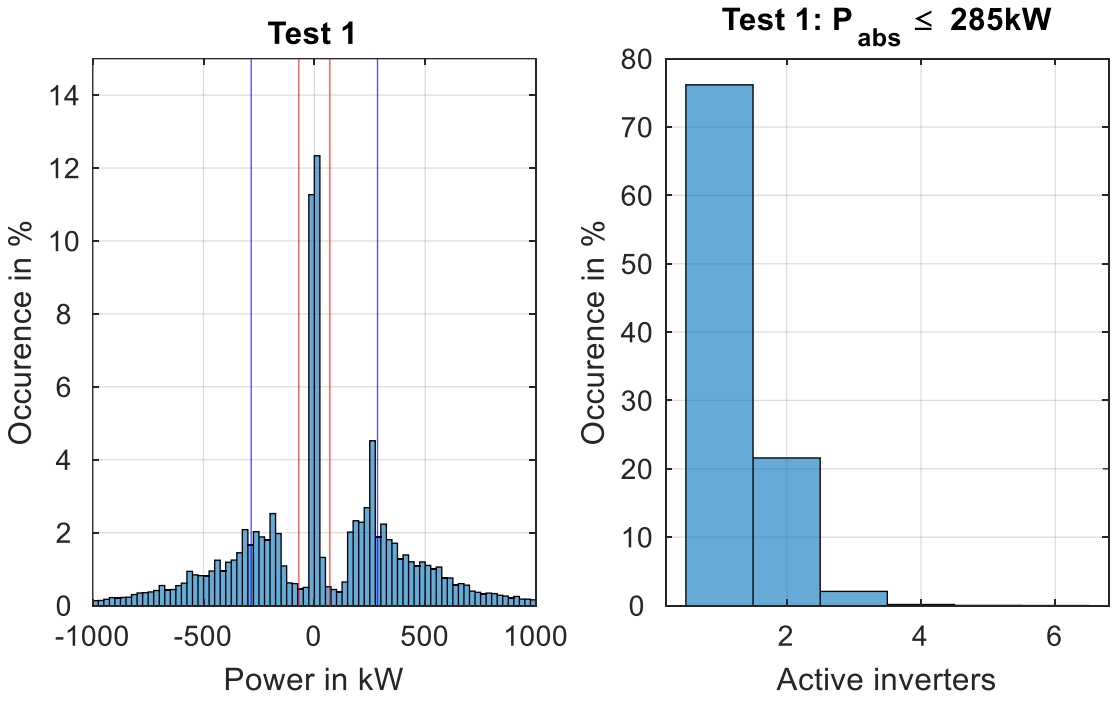

Figure 13: Left: Histogram of the requested power of the BESS for Test 1. Blue line: Inverter hysteresis power. Red line: Stage 1 power. Right: Histogram of the active inverters for an absolute power request of $P_{abs} \leq 285kW$

The histograms for all other testing procedures are shown in the appendix in Figure 18. The distributions are comparable to the distribution shown in Figure 13. It can therefore be seen that most power requests can be met by only one battery unit, and the inverter hysteresis power has a negligible influence on those power requests.

Power distributions for all battery units and all tests can be found in Figure 17 in the appendix. Those distributions are intended to represent the inverter hysteresis powers within the global efficiency options. The lithium-ion batteries experience higher power than the lead-acid batteries due to the lower power capabilities of the lead-acid batteries. In addition, the mean values of the lead-acid batteries are often shifted to the negative, which means that the lead-acid batteries have to be charged more frequently due to their lower efficiency. The boxes of the boxplots are all within $\pm 200\ kW$ despite different inverter hysteresis power settings.

5.2 Benchmark – full load cycle

As a reference measurement, a full cycle with the maximum possible power output is performed with two battery units which are connected to one transformer. All other inverters were shut down for this test, and the idle losses of the other transformers were calculated to correct the efficiency values by those idle losses.

In Figure 14, the measured power output for the full load test is shown. When the battery units reach low or high SOC states, the power output is limited to prevent any battery damage. A positive power value corresponds to a discharging process of the battery units, while negative power values correspond to a charging procedure of the battery units.

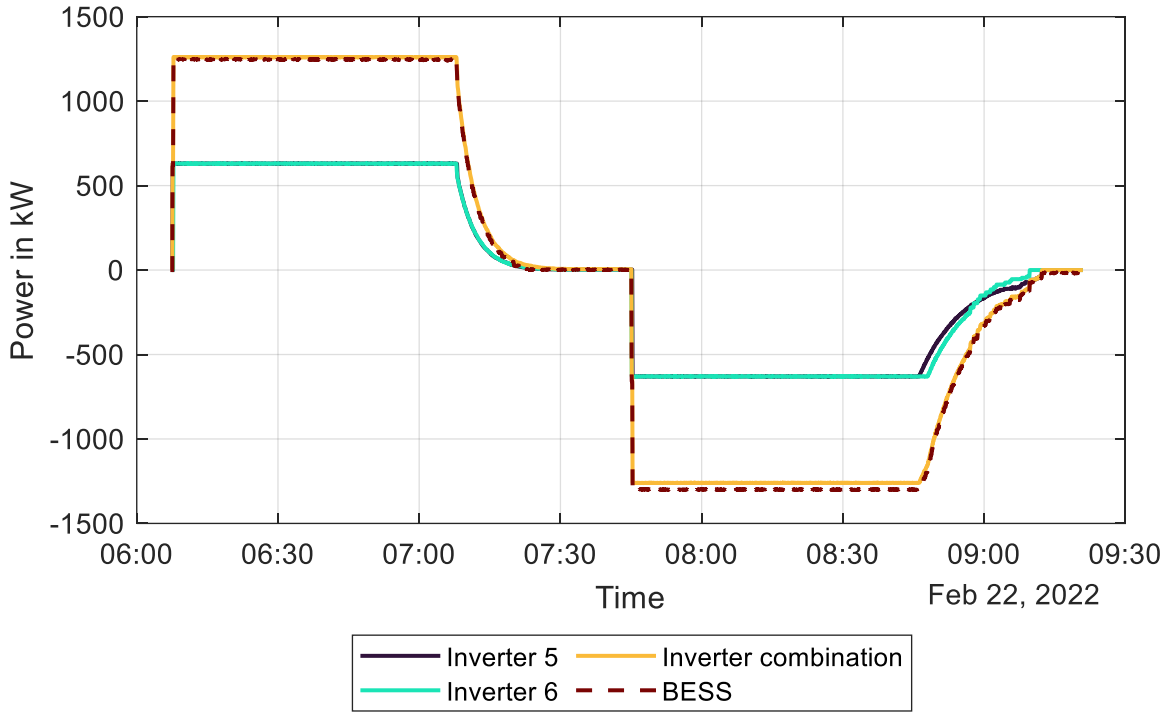

Figure 14: Measured power output for the full load test procedure. Note: Battery discharging corresponds to a positive power, while charging corresponds to a negative power.

From the performed full cycle of the battery units, the efficiency is calculated for each component. In Table 8, the results are listed. The inverter combination from Figure 14 is stated as aggregated inverter in Table 8, and the addition of both battery units is stated as aggregated battery. Like before, the BESS remains the measurement at the grid node.

Table 8: Round-trip-efficiencies for the whole BESS and its components. The measurements are done with one transformer and two inverters & battery combinations connected to this transformer. All other batteries and inverters were turned off for this test.

Component	Round-trip-efficiency in %
BESS	87.95
Transformer	96.92
Inverter (aggregated)	94.81
Battery (aggregated)	95.71

The values from Table 8 are referenced as Test X in section 5.3 and represent the benchmark and maximum possible efficiency for the BESS. At this point, it must be mentioned that the efficiencies of individual components, such as the batteries or inverters, may be higher in other tests due to lower utilization rates. However, the BESS efficiency of 87.95 % cannot be exceeded for the BESS M5BAT.

5.3 Efficiencies

In this section, the efficiencies of the components are analyzed. Comparative values from 2021, 2022, the benchmark test and the mean value of the SPDA V.2022[12] are always shown. Although the values for 2021 and 2022 include all operational tests, tests for research projects, and maintenance, the changed values provide an indicator of the current development of the efficiencies.

The overall round-trip-efficiency for the BESS is Figure 15 while for the components (transformer, inverter, battery) the losses are shown in Figure 15. The losses and efficiency always add up to 100 %. The component efficiencies can be found in the appendix in Figure 19.

[12] mean value of test 2 to test 5 from [17].

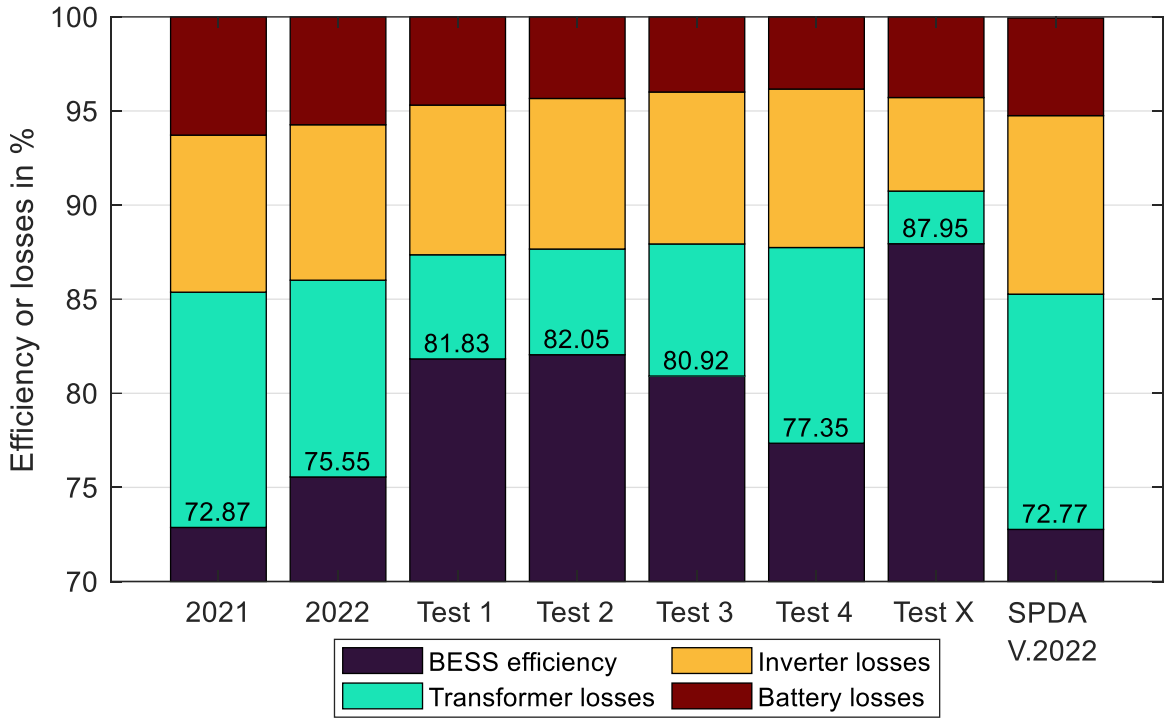

Figure 15: Round trip efficiency of the BESS and component losses for all testing procedures.

5.3.1 Battery efficiency

In this section, the BESS battery energy efficiency is examined in the different test scenarios. The round-trip efficiency (RTE) for the BESS batteries is between 95 % and 96 % for all testing procedures and can be found in Figure 19 and in Figure 15 as losses. The benchmark set by test X is set to 95.71 % with only LMO batteries. The range of the efficiency variation of the BESS battery is with only about 1 % very low. The RTE for the BESS battery has two main dependencies: On the one hand, the usage of lithium-ion batteries and, on the other hand the C-rate of the batteries. Lithium-ion batteries have higher efficiencies than lead acid batteries (see section 2.2 and [65]). Thus, higher usage of lithium-ion batteries automatically results in higher RTE for the BESS battery. In addition, the efficiency slightly increases with lower C-rates of the individual batteries. Both effects have an influence on the BESS battery RTE. In comparison to the benchmark, test X overall on the batteries side, the efficiency cannot be improved more than a few percent-points.

5.3.2 Inverter efficiency

The inverter efficiency is strongly dependent on the use or the operating point of the inverter. The inverter efficiency area is shown in Figure 9. In Figure 15 the inverter losses for the different tests are compared, while the efficiencies are presented in Figure 19. The efficiency of the benchmark test X is around 4 % higher than for the regular-use scenarios. The mean inverter efficiency of test 1 to test 4 is compared to the SPDA V.2022 mean value, improved by 1 %.

With reference to the efficiency curve from Figure 9 and test X, the inverters in this test had a higher load, which led to a higher efficiency. Since the efficiency in all other tests lies around 91.5 %, it can be assumed that the average load is lower than 10 % of the nominal load and that the different settings of the inverter hysteresis power have no significant influence on the efficiency. Only the inverter threshold of 70 kW, which corresponds to about 11 % of the nominal power, ensures a minimum load of about 11 % of the inverters. All power requirements below 70 kW are still fulfilled, but there is no distribution of the power to different inverters.

5.3.3 Transformer efficiency

In addition to the inverters, the transformers have a major impact on system efficiency. By using battery units on the same transformer, the transformer use of the individual transformers can be increased. A higher inverter hysteresis power (see Table 6) therefore, means a greater target use of the transformers. The transformer efficiencies for the performed tests are presented in Figure 19 while Figure 15 shows the transformer losses. The efficiency in test X reaches to nearly 97 %, which meets the nominal efficiency of the datasheet. All other measured transformer efficiencies fall behind by up to 4 %-points. The variation of the transformer losses in Figure 15 reveals that the transformers and their utilization have the biggest impact on the BESS efficiency. The transformer efficiency of the SPDA V.2023 tests is compared to the year 2021 and the SPDA V.2022 mean value increased by about 3 %. This indicates the influence of the PDA on the efficiency and the improvements gained by the development od the SPDA V.2023.

5.3.4 Overall efficiency

For the overall system efficiency, the component losses subtract from 100 % to the BESS efficiencies in Figure 15. Since the battery units and inverters only differ by a few percentage points in the various tests, these components do not have a major effect on the system efficiency. However, the observed pattern from the transformer efficiency analysis is still visible. The benchmark test X shows with 88 % the highest system efficiency. The efficiency results from test 1 to test 3 are all in the region of 81 % to 82 %, while the efficiency in test 4 is with 77 % noticeable lower. The difference between those tests are the different inverter hysteresis settings. A wider band for the inverter hysteresis settings can be stated as beneficial for the overall efficiency. Compared to the 2021, 2022 and the SPDA V.2022 efficiency values, all tested efficiencies are significantly higher. This underlines that just software improvements on the PDA and EMS improve the economics in terms of the efficiency of a modular battery storage system.

6 Conclusion

A PDA must be included in the EMS in each modular BESS to control the power flows of the battery units. In this study, several effects of the presented SPDA V.2023 were demonstrated. Stage 1 for low power outputs leads to significantly less inverter switching behavior which minimizes time delays in the power output and is beneficial for the inverters. The desired SOC bands could still be maintained by the SPDA V.2023, and user-generated energy throughput patterns could be achieved by stage 2b, the energy throughput balancing of the SPDA V.2023. Thus, aging can be influenced by the choice of SOC bands and energy throughput by user inputs. According to the PCS efficiency calculations, the inverter hysteresis could be adjusted for the optimal efficiency range. The BESS efficiency could be increased to 80 % - 82 % compared to 73 % from 2017 to 2021 with the changes in the PDA and global efficiency options [51]. These software-only improvements to the BESS are not only relevant to the BESS M5BAT but can also be implemented in other hybrid BESS. In this way, the economic efficiency of BESS is improved while at the same time the aging parameters are optimized for the technology, which is of particular interest to BESS operators.

The controller at the grid connection point offers further potential for optimization by ensuring that the target and actual outputs match as closely as possible. The control behavior can be improved and possibly also influences the system efficiency. A further increase in efficiency and, thus the cost-effectiveness of BESS is only possible through an alternative hardware-based system layout and an increase in utilization through multi-use operation or single-use energy trading for arbitrage purposes. In addition, the benchmark test has shown that the efficiency of the transformers and inverters can be significantly increased (RTE 88 %) with an increased utilization of these components.

7 Acknowledgements

The research was supported by the German Federal Ministry of Economic Affairs and Climate Action (BMWK) and by the project partner Uniper SE as part of the public project M5BAT (Funding Code: 03ESP265F) and EMMUseBat (Funding Code: 03EI4034).

8 Author contributions

Lucas Koltermann: Conceptualization, Methodology, Software, Validation, Formal Analysis, Investigation, Data Curation, Visualization, Writing - Original Draft

Mauricio Celi Cortés: Software, Validation, Writing - Review & Editing

Jan Figgener: Conceptualization, Validation, Writing - Review & Editing, Supervision

Sebastian Zurmühlen: Validation, Writing - Review & Editing, Project administration, Funding acquisition

Dirk Uwe Sauer: Validation, Resources, Writing - Review & Editing, Supervision, Funding acquisition

9 References

[1] M. Schoenfisch and A. Dasgupta, "Grid-Scale Storage," Paris, 2022. [Online]. Available: https://www.iea.org/reports/grid-scale-storage

[2] J. Figgener *et al.,* "The development of battery storage systems in Germany: A market review (status 2023)," 2023, doi: 10.48550/arXiv.2203.06762.

[3] J. Figgener *et al.,* "The development of stationary battery storage systems in Germany – A market review," *Journal of Energy Storage*, vol. 29, p. 101153, 2020, doi: 10.1016/j.est.2019.101153.

[4] J. Figgener *et al.,* "The development of stationary battery storage systems in Germany – status 2020," *Journal of Energy Storage*, vol. 33, p. 101982, 2021, doi: 10.1016/j.est.2020.101982.

[5] J. Figgener *et al.,* "The development of battery storage systems in Germany: A market review (status 2022)," 2022, doi: 10.48550/arXiv.2203.06762.

[6] The International Renewable Energy Agency (IRENA), "Behind-The-Meter Batteries – Innovation Landscape Brief," IRENA, Abu Dhabi, 2019. Accessed: Jul. 29 2022. [Online]. Available: https://www.irena.org/-/media/Files/IRENA/Agency/Publication/2019/Sep/IRENA_BTM_Batteries_2019.pdf

[7] F. Karoui, D.-L. Ha, T. Delaplagne, M.-F. Bouaaziz, V. Eudier, and M. Lévy, "Diagnosis and prognosis of complex energy storage systems: tools development and feedback on four installed systems," *Energy Procedia*, vol. 155, pp. 61–76, 2018, doi: 10.1016/j.egypro.2018.11.066.

[8] M. Dubarry, M. Tun, G. Baure, M. Matsuura, and R. E. Rocheleau, "Battery Durability and Reliability under Electric Utility Grid Operations: Analysis of On-Site Reference Tests," *Electronics*, vol. 10, no. 13, p. 1593, 2021, doi: 10.3390/electronics10131593.

[9] M. Swierczynski, D.-I. Stroe, A.-I. Stan, R. Teodorescu, R. Laerke, and P. C. Kjaer, "Field tests experience from 1.6MW/400kWh Li-ion battery energy storage system providing primary frequency regulation service," in *IEEE PES ISGT Europe 2013*, Lyngby, Denmark, Oct. 2013 - Oct. 2013, pp. 1–5.

[10] L. Lo Schiavo and M. Benini, "Pilot projects on Battery Energy Storage Systems in the Transmission grid: regulatory framework and first results," in *2018 AEIT International Annual Conference (AEIT): Bari (Italy), October 3-5, 2018*, 2018, pp. 1–6.

[11] M. Koller, T. Borsche, A. Ulbig, and G. Andersson, "Review of grid applications with the Zurich 1MW battery energy storage system," *Electric Power Systems Research*, vol. 120, pp. 128–135, 2015, doi: 10.1016/j.epsr.2014.06.023.

[12] L. Consiglio, G. Di Lembo, C. Noce, P. Eckert, A. Rasic, and A. Schuette, "Performances of the first electric storage system of Enel Distribuzione," in *22nd International*

Conference and Exhibition on Electricity Distribution (CIRED 2013), Stockholm, Sweden, Jun. 2013, pp. 1–5.

[13] L. Koltermann *et al.,* "Potential analysis of current battery storage systems for providing fast grid services like synthetic inertia – Case study on a 6 MW system," *Journal of Energy Storage*, vol. 57, p. 106190, 2023, doi: 10.1016/j.est.2022.106190.

[14] B. Gundogdu, S. Nejad, D. T. Gladwin, and D. A. Stone, "A battery energy management strategy for UK enhanced frequency response," pp. 26–31, 2020, doi: 10.1109/ISIE.2017.8001218.

[15] T. Thien, D. Schweer, D. vom Stein, A. Moser, and D. U. Sauer, "Real-world operating strategy and sensitivity analysis of frequency containment reserve provision with battery energy storage systems in the german market," *Journal of Energy Storage*, vol. 13, pp. 143–163, 2017, doi: 10.1016/j.est.2017.06.012.

[16] J. Münderlein, M. Steinhoff, S. Zurmühlen, and D. U. Sauer, "Analysis and evaluation of operations strategies based on a large scale 5 MW and 5 MWh battery storage system," *Journal of Energy Storage*, vol. 24, p. 100778, 2019, doi: 10.1016/j.est.2019.100778.

[17] L. Koltermann, K. Jacqué, J. Figgener, S. Zurmühlen, and D. U. Sauer, "Operational Validation of a Power Distribution Algorithm for a Modular Megawatt Battery Storage System," *Batteries & Supercaps*, vol. 6, no. 3, 2023, doi: 10.1002/batt.202200414.

[18] T. Thien, H. Axelsen, M. Merten, and D. U. Sauer, "Energy management of stationary hybrid battery energy storage systems using the example of a real-world 5 MW hybrid battery storage project in Germany," *Journal of Energy Storage*, vol. 51, p. 104257, 2022, doi: 10.1016/j.est.2022.104257.

[19] J. Münderlein, G. Ipers, M. Steinhoff, S. Zurmühlen, and D. U. Sauer, "Optimization of a hybrid storage system and evaluation of operation strategies," *International Journal of Electrical Power & Energy Systems*, vol. 119, p. 105887, 2020, doi: 10.1016/j.ijepes.2020.105887.

[20] K. Jacqué, L. Koltermann, J. Figgener, S. Zurmühlen, and D. U. Sauer, "The Influence of Frequency Containment Reserve on the Operational Data and the State of Health of the Hybrid Stationary Large-Scale Storage System," *Energies*, vol. 15, no. 4, p. 1342, 2022, doi: 10.3390/en15041342.

[21] R. H. Byrne, T. A. Nguyen, D. A. Copp, B. R. Chalamala, and I. Gyuk, "Energy Management and Optimization Methods for Grid Energy Storage Systems," *IEEE Access*, vol. 6, pp. 13231–13260, 2018, doi: 10.1109/ACCESS.2017.2741578.

[22] H. Shafique, L. B. Tjernberg, D.-E. Archer, and S. Wingstedt, "Energy Management System (EMS) of Battery Energy Storage System (BESS) – Providing Ancillary Services," in *2021 IEEE Madrid PowerTech: Conference proceedings*, Piscataway, NJ: IEEE, 2021, pp. 1–6.

[23] X. Li and D. Zhang, "Coordinated Control and Energy Management Strategies for Hundred Megawatt-level Battery Energy Storage Stations Based on Multi-agent Theory," in *2018 International Conference on Advanced Mechatronic Systems: August 30-September 2, 2018, Zhengzhou, China*, IEEE, Ed., Piscataway, NJ: IEEE, 2018, pp. 1–5.

[24] L. Ngoc An and T. Quoc-Tuan, "Optimal energy management for grid connected microgrid by using dynamic programming method," in *IEEE Power & Energy Society general meeting, 2015: 26 - 30 July 2015, Denver, CO, USA*, Piscataway, NJ: IEEE, 2015, pp. 1–5.

[25] V. V. Babu, J. Preetha Roselyn, and P. Sundaravadivel, "Multi-objective genetic algorithm based energy management system considering optimal utilization of grid and degradation of battery storage in microgrid," *Energy Reports*, vol. 9, pp. 5992–6005, 2023, doi: 10.1016/j.egyr.2023.05.067.

[26] J. Marchgraber, W. Gawlik, and G. Wailzer, "Reducing SoC-Management and losses of battery energy storage systems during provision of frequency containment reserve," *Journal of Energy Storage*, vol. 27, p. 101107, 2020, doi: 10.1016/j.est.2019.101107.

[27] J.-Y. Choi, I.-S. Choi, G.-H. Ahn, and D.-J. Won, "Advanced Power Sharing Method to Improve the Energy Efficiency of Multiple Battery Energy Storages System," *IEEE Trans. Smart Grid*, vol. 9, no. 2, pp. 1292–1300, 2018, doi: 10.1109/TSG.2016.2582842.

[28] M. Mühlbauer, O. Bohlen, and M. A. Danzer, "Analysis of power flow control strategies in heterogeneous battery energy storage systems," *Journal of Energy Storage*, vol. 30, p. 101415, 2020, doi: 10.1016/j.est.2020.101415.

[29] M. Mühlbauer, S. Klier, H. Palm, O. Bohlen, and M. A. Danzer, "A Novel Power Flow Control Strategy for Heterogeneous Battery Energy Storage Systems Based on Prognostic Algorithms for Batteries," pp. 1–11, 2020, doi: 10.23919/EPE20ECCEEurope43536.2020.9215818.

[30] M. Mühlbauer, F. Rang, H. Palm, O. Bohlen, and M. A. Danzer, "Pareto-optimal power flow control in heterogeneous battery energy storage systems," *Journal of Energy Storage*, vol. 48, p. 103803, 2022, doi: 10.1016/j.est.2021.103803.

[31] T. Rüther, P. Mößle, M. Mühlbauer, O. Bohlen, and M. A. Danzer, "Iterative Dynamic Programming—An Efficient Method for the Validation of Power Flow Control Strategies," *Electricity*, vol. 3, no. 4, pp. 542–562, 2022, doi: 10.3390/electricity3040027.

[32] S.-M. Cho and S.-Y. Yun, "Optimal Power Assignment of Energy Storage Systems to Improve the Energy Storage Efficiency for Frequency Regulation," *Energies*, vol. 10, no. 12, p. 2092, 2017, doi: 10.3390/en10122092.

[33] M. Schimpe, C. Piesch, H. Hesse, J. Paß, S. Ritter, and A. Jossen, "Power Flow Distribution Strategy for Improved Power Electronics Energy Efficiency in Battery Storage

Systems: Development and Implementation in a Utility-Scale System," *Energies*, vol. 11, no. 3, p. 533, 2018, doi: 10.3390/en11030533.

[34] J. W. Stevens and G. P. Corey, "A study of lead-acid battery efficiency near top-of-charge and the impact on PV system design," pp. 1485–1488, 1996, doi: 10.1109/PVSC.1996.564417.

[35] E. D. Sexton and J. B. Olson, "Coulombic efficiency of a sealed, thin plate, spiral lead-acid battery," pp. 297–301, 1998, doi: 10.1109/BCAA.1998.653883.

[36] T. Le Varlet, O. Schmidt, A. Gambhir, S. Few, and I. Staffell, "Comparative life cycle assessment of lithium-ion battery chemistries for residential storage," *Journal of Energy Storage*, vol. 28, p. 101230, 2020, doi: 10.1016/j.est.2020.101230.

[37] M. Elliott, L. G. Swan, M. Dubarry, and G. Baure, "Degradation of electric vehicle lithium-ion batteries in electricity grid services," *Journal of Energy Storage*, vol. 32, p. 101873, 2020, doi: 10.1016/j.est.2020.101873.

[38] B. Ellis, C. White, and L. Swan, "Degradation of lithium-ion batteries that are simultaneously servicing energy arbitrage and frequency regulation markets," *Journal of Energy Storage*, vol. 66, p. 107409, 2023, doi: 10.1016/j.est.2023.107409.

[39] K. Li and K. J. Tseng, "Energy efficiency of lithium-ion battery used as energy storage devices in micro-grid," pp. 5235–5240, doi: 10.1109/IECON.2015.7392923.

[40] E. Redondo-Iglesias, P. Venet, and S. Pelissier, "Efficiency Degradation Model of Lithium-Ion Batteries for Electric Vehicles," *IEEE Trans. on Ind. Applicat.*, vol. 55, no. 2, pp. 1932–1940, 2019, doi: 10.1109/TIA.2018.2877166.

[41] E. Redondo-Iglesias and S. Pelissier, "On the Efficiency of LFP Lithium-ion Batteries," in *2022 Second International Conference on Sustainable Mobility Applications, Renewables and Technology (SMART): November 23-25, 2022*, 2022, pp. 1–5.

[42] M. Dubarry and A. Devie, "Battery durability and reliability under electric utility grid operations: Representative usage aging and calendar aging," *Journal of Energy Storage*, vol. 18, pp. 185–195, 2018, doi: 10.1016/j.est.2018.04.004.

[43] J. M. Reniers and D. A. Howey, "Digital twin of a MWh-scale grid battery system for efficiency and degradation analysis," *Applied Energy*, vol. 336, p. 120774, 2023, doi: 10.1016/j.apenergy.2023.120774.

[44] P. Keil *et al.,* "Calendar Aging of Lithium-Ion Batteries," *J. Electrochem. Soc.*, vol. 163, no. 9, A1872-A1880, 2016, doi: 10.1149/2.0411609jes.

[45] J. Schmalstieg, S. Käbitz, M. Ecker, and D. U. Sauer, "A holistic aging model for Li(NiMnCo)O2 based 18650 lithium-ion batteries," *Journal of Power Sources*, vol. 257, pp. 325–334, 2014, doi: 10.1016/j.jpowsour.2014.02.012.

[46] T. Bank, J. Feldmann, S. Klamor, S. Bihn, and D. U. Sauer, "Extensive aging analysis of high-power lithium titanate oxide batteries: Impact of the passive electrode effect,"

Journal of Power Sources, vol. 473, p. 228566, 2020, doi: 10.1016/j.jpowsour.2020.228566.

[47] M. Franke and J. Kowal, "Empirical sulfation model for valve-regulated lead-acid batteries under cycling operation," *Journal of Power Sources*, vol. 380, pp. 76–82, 2018, doi: 10.1016/j.jpowsour.2018.01.053.

[48] L. Wildfeuer, A. Karger, D. Aygül, N. Wassiliadis, A. Jossen, and M. Lienkamp, "Experimental degradation study of a commercial lithium-ion battery," *Journal of Power Sources*, vol. 560, p. 232498, 2023, doi: 10.1016/j.jpowsour.2022.232498.

[49] J. Münderlein, M. Steinhoff, H. Axelsen, and D. U. Sauer, "Planning, building, efficiency measurement and determination of forecast data of a grid-scale hybrid 5 MW / 5 MWh battery storage system," in *2017 IEEE International Telecommunications Energy Conference (INTELEC)*, Broadbeach, QLD, Oct. 2017 - Oct. 2017, pp. 314–320.

[50] K. Jacqué, L. Koltermann, J. Figgener, S. Zurmühlen, and D. U. Sauer, "The influence of frequency containment reserve on the cycles of a hybrid stationary large-scale storage system," *Journal of Energy Storage*, vol. 52, p. 105040, 2022, doi: 10.1016/j.est.2022.105040.

[51] K. Jacqué, L. Koltermann, J. Figgener, S. Zurmühlen, and D. U. Sauer, "The influence of frequency containment reserve on the efficiency of a hybrid stationary large-scale storage system," *Journal of Energy Storage*, vol. 52, p. 104961, 2022, doi: 10.1016/j.est.2022.104961.

[52] L. Koltermann, M. Celi Cortés, J. Figgener, S. Zurmühlen, and D. U. Sauer, "Power curves of megawatt-scale battery storage technologies for frequency regulation and energy trading," *Applied Energy*, vol. 347, p. 121428, 2023, doi: 10.1016/j.apenergy.2023.121428.

[53] Institute for Power Generation and Storage Systems (RWTH Aachen), "Modularer multi-Megawatt multi-Technologie Mittelspannungs-Batteriespeicher (M5BAT): Abschlussbericht, Datenblätter sowie weiteres Aktenarchiv," Förderkennzeichen: 03ESP265A, 2019.

[54] *Commission Regulation (EU) 2017/2195 of 23 November 2017 establishing a guideline on electricity balancing: EB-GL*, 2017. Accessed: Dec. 3 2021. [Online]. Available: https://eur-lex.europa.eu/legal-content/EN/TXT/PDF/?uri=CELEX:32017R2195&from=EN

[55] X. Luo *et al.,* "Review of Voltage and Frequency Grid Code Specifications for Electrical Energy Storage Applications," *Energies*, vol. 11, no. 5, p. 1070, 2018, doi: 10.3390/en11051070.

[56] 50Hertz Transmission GmbH, Amprion GmbH, TenneT TSO GmbH, and TransnetBW GmbH, "Prequalification Process for Balancing Service Providers (FCR, aFRR, mFRR) in Germany ("PQ conditions")," May. 2020. Accessed: Feb. 10 2022. [Online].

Available: https://www.regelleistung.net/ext/download/PQ_Bedingungen_FCR_aFRR_mFRR_en

[57] 50Hertz Transmission GmbH, Amprion GmbH, TenneT TSO GmbH, and TransnetBW GmbH, "Eckpunkte und Freiheitsgrade bei Erbringung von Primärregelleistung," [Online]. Available: https://www.regelleistung.net/

[58] L. Koltermann, K. Jacqué, J. Figgener, S. Zurmühlen, and D. Uwe Sauer, "Balancing group deviation & balancing energy costs due to the provision of frequency containment reserve with a battery storage system in Germany," *International Journal of Electrical Power & Energy Systems*, vol. 142, p. 108327, 2022, doi: 10.1016/j.ijepes.2022.108327.

[59] Hamed Amini, *area_stairs*: MATLAB Central File Exchange, 2023. Accessed: May 16 2023. [Online]. Available: https://www.mathworks.com/matlabcentral/fileexchange/32267-area_stairs

[60] J. Schneider Elektrotechnik GmbH, "Technisches Datenblatt: HSGX 1260F-1605T06001 Dreiphasen - Hochspannungstransformator," Feb. 2016.

[61] SMA Solar Technology AG, "Datenblatt - SUNNY CENTRAL STORAGE 500 / 630 / 720 / 760 / 800 / 850 / 900 / 1000," 2016. [Online]. Available: https://files.sma.de/downloads/SCS500-1000-DDE1610-V21web.pdf

[62] SMA Solar Technology AG, "Betriebsanleitung: SUNNY CENTRAL STORAGE 500 / 630 / 720 / 760 / 800 / 850 / 900 / 1000," 2016. [Online]. Available: https://files.sma.de/downloads/SCS-BE-E7-de-12.pdf

[63] D. U. Sauer and H. Schmidt, "Praxisgerechte Modellierung und Abschätzung von Wechselrichter Wirkungsgraden," in *9. Internationales Sonnenforum*, 1994, pp. 550–557. [Online]. Available: https://publications.rwth-aachen.de/record/761388

[64] A. Danz, *boxplotGroup*: MATLAB Central File Exchange, 2022. Accessed: Jul. 27 2022. [Online]. Available: https://de.mathworks.com/matlabcentral/fileexchange/74437-boxplotgroup

[65] A.-I. Stan, M. Swierczynski, D.-I. Stroe, R. Teodorescu, S. J. Andreasen, and K. Moth, "A comparative study of lithium ion to lead acid batteries for use in UPS applications," in *2014 IEEE 36th International Telecommunications Energy Conference (INTELEC 2014): Vancouver, British Columbia, Canada, 28 September - 2 October 2014*, Piscataway, NJ: IEEE, 2014, pp. 1–8.

10 Appendix

Figure 16 shows the combination of inverter and transformer losses in different activation settings. The outer curves mark the configuration with the highest and lowest losses. With the SPDA V.2023 the objective is to come as close as possible to the configuration with the lowest losses.

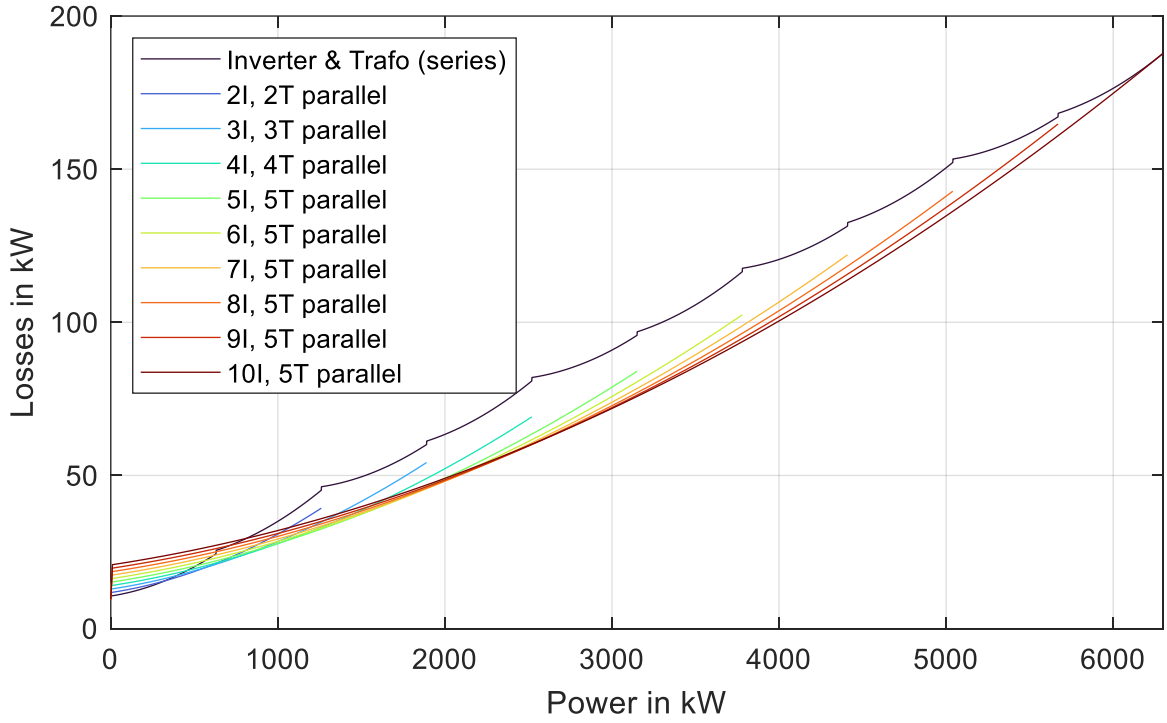

Figure 16: Transformer (T) and inverter (I) losses combined.

The power distribution is presented in Figure 17.

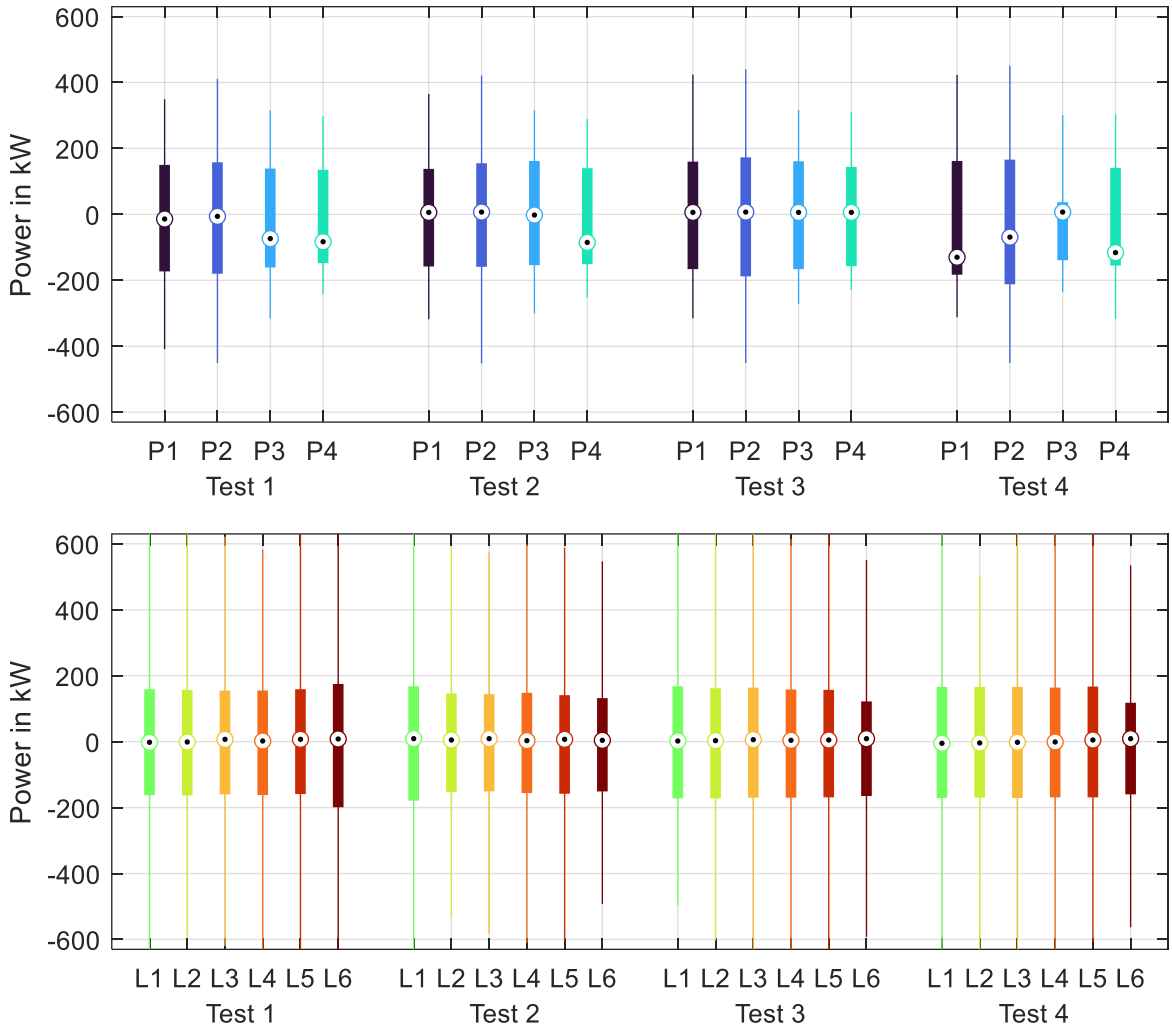

Figure 17: Boxplots of the power distribution for each battery unit of M5BAT. The upper subplot shows the lead-acid batteries, while the lower subplot shows the Lithium batteries with the shortened acronyms according to Table 2 [64].

In Figure 18, histograms with the power request distribution for the BESS are shown for each test. The blue lines mark the inverter hysteresis power setting, while the red lines mark the stage 1 power setting. All power requests between the red lines must be fulfilled by only one battery unit, and all power requests between the red and blue lines can be fulfilled by one battery unit. It can therefore be seen that most power requests can be met by only one battery unit, and the inverter hysteresis power has no influence on those power requests.

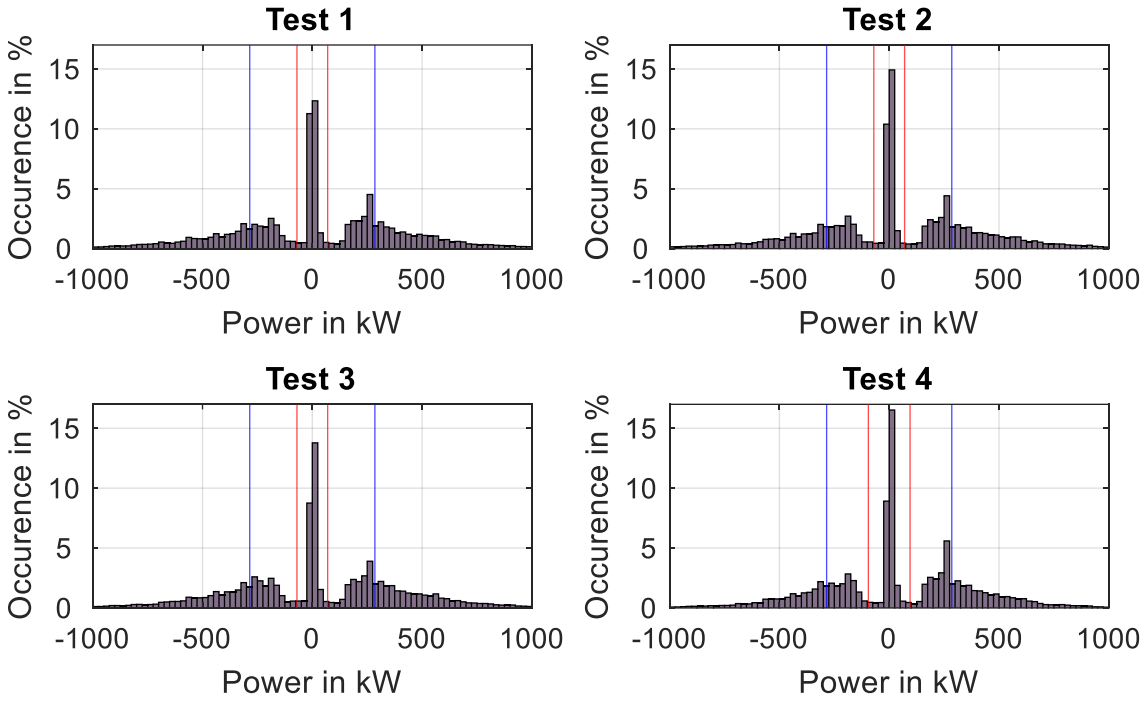

Figure 18: Histograms of the requested power of the BESS. Blue line: Inverter hysteresis power. Red line: Stage 1 power

In Figure 19 the efficiencies for all components in all test procedures are shown. The battery efficiency is stable throughout all tests. The inverter efficiency is slightly over 91 % except for the benchmark test, where a higher efficiency is reached. The transformer efficiency varies a lot stronger than all other efficiencies.

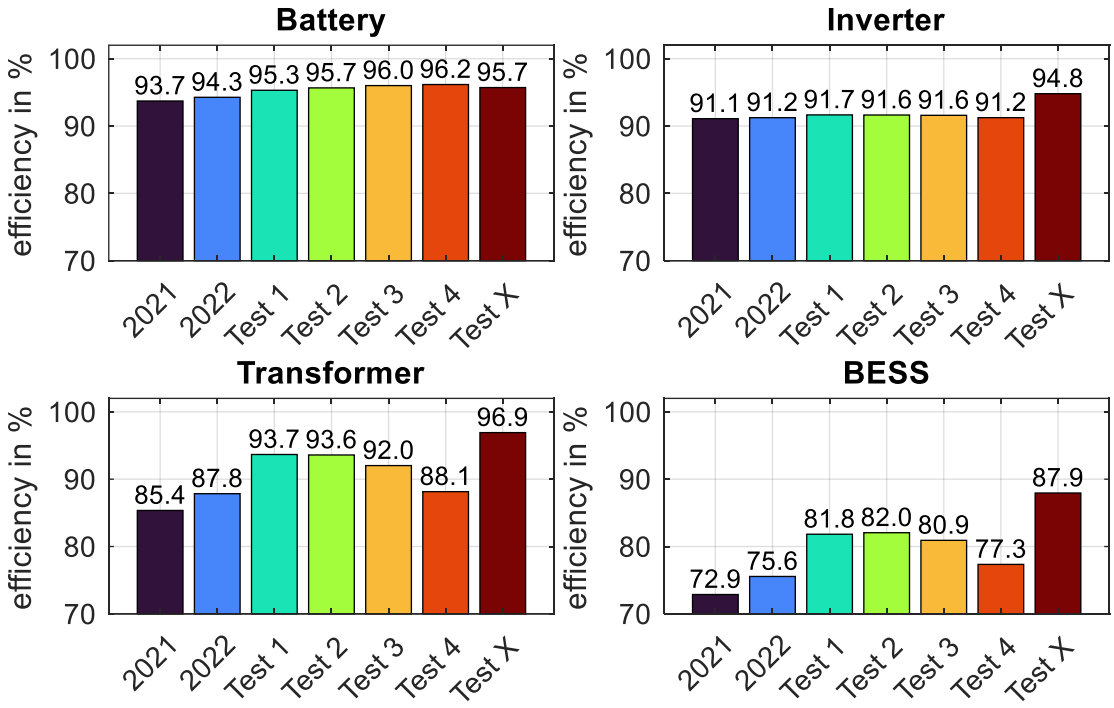

Figure 19: Round-trip-efficiency for all components of the BESS individual and BESS round-trip-efficiency.